water

MDPI

Article

The Effects of Climate Change on Streamflow, Nitrogen Loads, and Crop Yields in the Gordes Dam Basin, Turkey

Ayfer Özdemir [1,2,*], Martin Volk [2,*], Michael Strauch [2] and Felix Witing [2]

[1] West Mediterranean Agricultural Research Institute, Republic of Turkey Ministry of Agriculture and Forestry, Boztepe Mah. Serik Caddesi no:270, 07110 Aksu, Antalya, Turkey
[2] Helmholtz Centre for Environmental Research—UFZ, Department of Computational Landscape Ecology, Permoserstr. 15, 04318 Leipzig, Germany; michael.strauch@ufz.de (M.S.)
* Correspondence: ozdemir.ayfer@tarimorman.gov.tr or ozdemir.ayfer@gmail.com (A.Ö.); martin.volk@ufz.de (M.V.)

Abstract: The Mediterranean region is highly vulnerable to climate change. Longer and more intense heatwaves and droughts are expected. The Gordes Dam in Turkey provides drinking water for Izmir city and irrigation water for a wide range of crops grown in the basin. Using the Soil and Water Assessment Tool (SWAT), this study examined the effects of projected climate change (RCP 4.5 and RCP 8.5) on the simulated streamflow, nitrogen loads, and crop yields in the basin for the period of 2031–2060. A hierarchical approach to define the hydrological response units (HRUs) of SWAT and the Fast Automatic Calibration Tool (FACT) were used to reduce computational time and improve model performance. The simulations showed that the average annual discharge into the reservoir is projected to increase by between 0.7 m^3/s and 4 m^3/s under RCP 4.5 and RCP 8.5 climate change scenarios. The steep slopes and changes in precipitation in the study area may lead to higher simulated streamflow. In addition, the rising temperatures predicted in the projections could lead to earlier spring snowmelt. This could also lead to increased streamflow. Projected nitrogen loads increased by between 8.8 and 25.1 t/year. The results for agricultural production were more variable. While the yields of poppy, tobacco, winter barley, and winter wheat will increase to some extent because of climate change, the yields of maize, cucumbers, and potatoes are all predicted to be negatively affected. Non-continuous and limited data on water quality and crop yields lead to uncertainties, so that the accuracy of the model is affected by these limitations and inconsistencies. However, the results of this study provide a basis for developing sustainable water and land management practices at the catchment scale in response to climate change. The changes in water quality and quantity and the ecological balance resulting from changes in land use and management patterns for economic benefit could not be fully demonstrated in this study. To explore the most appropriate management strategies for sustainable crop production, the SWAT model developed in this study should be further used in a multi-criteria land use optimization analysis that considers not only crop yields but also water quantity and quality targets.

Keywords: climate change impact; river basin management; flow rate; nitrogen loads; crop yields

check for updates

Citation: Özdemir, A.; Volk, M.; Strauch, M.; Witing, F. The Effects of Climate Change on Streamflow, Nitrogen Loads, and Crop Yields in the Gordes Dam Basin, Turkey. *Water* **2024**, *16*, 1371. https://doi.org/10.3390/w16101371

Academic Editor: Athanasios Loukas

Received: 22 March 2024
Revised: 3 May 2024
Accepted: 8 May 2024
Published: 11 May 2024

Copyright: © 2024 by the authors. Licensee MDPI, Basel, Switzerland. This article is an open access article distributed under the terms and conditions of the Creative Commons Attribution (CC BY) license (https://creativecommons.org/licenses/by/4.0/).

1. Introduction

The Intergovernmental Panel on Climate Change [1] has stated that the concentration of greenhouse gases in the atmosphere will continue to increase due to the combined effects of natural factors and human activities, resulting in continued warming of the global climate system [2]. Changes in climate have already affected hydrology, water quality, agricultural production, and precipitation regimes and led to an increased frequency of extreme weather events such as droughts and floods in several regions of the world [3,4]. The Mediterranean is one of the most vulnerable regions [5] where significant decreases in precipitation and increases in temperature are expected [6–9]. According to the results of the RCP 4.5 and RCP 8.5 scenarios of the global circulation models HadGEM2-ES, MPI-ESM-MR, and GFDL-ESM2M, the mean temperature in Turkey is expected to increase by between 1 °C and 6 °C. Although there is no regular decreasing or increasing trend throughout the projection period, the irregularity of the precipitation regime is attracting more attention. For precipitation projections, according to RCP 4.5 in the period (2016–2040), there would be an increase of about 10–40% in precipitation during the winter months in the coastal part of the Aegean Sea. In the period of 2041–2070, according to RCP 8.5, there would be a decrease of about 50% in summer precipitation throughout the country, except for the western and eastern parts of the Black Sea, the coastal part of the Aegean Sea, and the Marmara region [10]. The high spatial and temporal climate variability in this region, characterized by complex mountain ranges, distinct basins, seas, bays, islands, and peninsulas of different sizes and with complex morphological features, makes it difficult to predict the impacts of climate change in the Gediz Basin [11–13]. The Gediz Basin is projected to experience mean annual temperature increases of 1.5 to 2.2 °C and mean annual total PET (potential evapotranspiration) increases of 5 to 8% [14,15]. Compared to the historical value, the ensemble of all climate projections also shows an expected increase in the mean annual inflow of +15.4% in the Demirkopru reservoir in the Gediz basin [16]. Freshwater demand for irrigated crops in the Mediterranean is expected to increase with climate change, exacerbating water stress [14]. Hydro-climatic changes are expected to have a negative impact on crop production and hydropower generation [6,17–19]. Agricultural research and development should develop cereal varieties that can tolerate high temperatures and rainfall intensity [20] to maintain production efficiency and resource allocation in the long term. The Gediz River Basin in western Turkey is already experiencing water scarcity and pollution due to rapid demographic and economic development, urbanization, industrialization, and inefficient irrigation [21,22]. These challenges are likely to be exacerbated by the effects of climate change. Agriculture is the main economic activity in the Gediz Basin. However, there are few studies in Turkey on the potential impacts of climate change on the ecosystems, hydrology, and socio-economy of watersheds. Such studies are necessary to develop appropriate water and land management strategies to cope with climate change.

The Soil and Water Assessment Tool (SWAT) is one of the most widely used hydrological models. It has been applied to simulate water quantity, quality, and crop yields in various watersheds [23,24], often with a particular focus on the impacts of climate change [2,3,25]. Although there are many studies undertaken to understand climate change impacts on streamflow, nitrogen loads, and crop yields, these impacts have been studied separately; climate change impacts on these parameters should be investigated together in the same study on the basin to provide integrated basin management. The smallest spatial unit of the model is called the hydrologic response unit (HRU). By default, HRUs in SWAT are generated by lumping all similar land uses, soils, and slopes within a subbasin, where the user can define thresholds for excluding land use, soil, and slope classes of smaller areas. A potential disadvantage of this is that some important combinations that may have a significant impact on hydrological processes in the watershed may be ignored if thresholds are chosen that are too high. On the other hand, if the applied thresholds are too low, the large number of HRUs will increase the computational time and thus may hinder sound model parameterization and calibration. To improve model performance and reduce computational complexity simultaneously, Ozdemir et al. (2017) [26] developed a hierarchical HRU division approach to simultaneously improve model performance and reduce computational time. This study first divides HRUs into two types and optimizes them with respect to some relevant parameters. Then, each HRU is divided into two further HRU types. Each of the child HRUs inherits the optimal values of the parameters of the parent HRU as its initial value. Two basins, namely the Sarisu-Eylikler and Namazgah Dam Lake basins in Turkey, were used to demonstrate the performance of the hierarchical methodology. In Sarisu-Eylikler, good results were obtained using a combination of curve number (CN2), soil hydraulic conductivity, and slope to generate HRUs. In Namazgah, using only CN2 gave better results.

In this study, we applied the hierarchical HRU partitioning approach to SWAT and used the model to simulate the effects of climate change on streamflow, nitrogen loads, and crop yields in the Gordes Dam Basin which is a sub-basin of the Gediz River Basin. The Gordes Dam Basin provides both drinking water for the city of Izmir and irrigation water for intensive crop production. The specific objectives of the study were (1) to apply a hierarchical HRU partitioning approach to SWAT to determine the optimal number of HRUs to reduce model computation time, (2) to quantify the effects of future climate change on streamflow, nitrogen loads, and crop yields in the Gordes Dam Basin for the period of 2031 to 2060, assuming two representative concentration pathway (RCP) emission scenarios, RCP 4. 5 and RCP 8.5, (3) to assess the impact of climate change on streamflow, nitrogen loads, and crop yields compared to the historical period. The results of the study can be used by decision-makers to develop climate change adaptation strategies for water and land management in the study region.

2. Materials and Methods

2.1. Study Area

The Gordes Dam is located between 39°10′–38°40′ north longitude and 28°5′ and 28°30′ east latitude in the Aegean region of Turkey (Figure 1). The dam was constructed at the Gordes River to provide irrigation water for the surrounding agricultural areas. The dam is also used to supply drinking water to Izmir province. It has an active storage volume of 5,500,000 m^3 and covers a surface area of 14.05 km^2 at the average water level. The basin area is 1050 km^2 with elevations ranging from 72 to 1540 m a.s.l. The recorded mean annual total for precipitation and potential evaporation are 613 mm and 744.3 mm, respectively. The mean annual maximum and minimum temperatures are 21.07 °C and 8.42 °C, respectively. The mean annual flow rate of the Gordes River is 2.64 m^3/s. The predominant soil types are lime-free brown forest soils and lime-free brown soils, which typically have a rather low water storage capacity and cover about 32% and 20% of the study area, respectively (Figure 2a). Land use in the basin is predominantly agriculture (45%), followed by coniferous forest (33%) (Figure 2b).

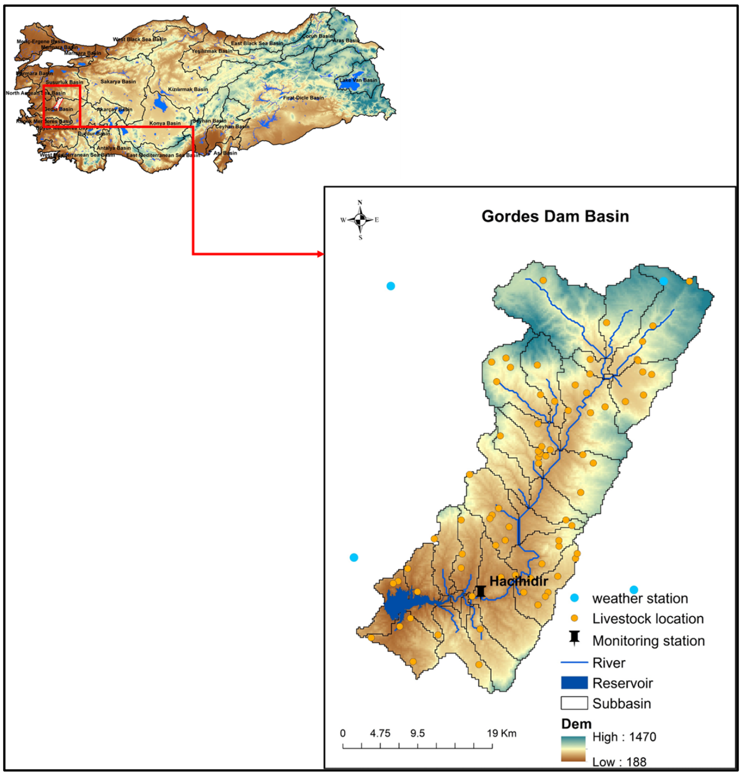

Figure 1. Study area.

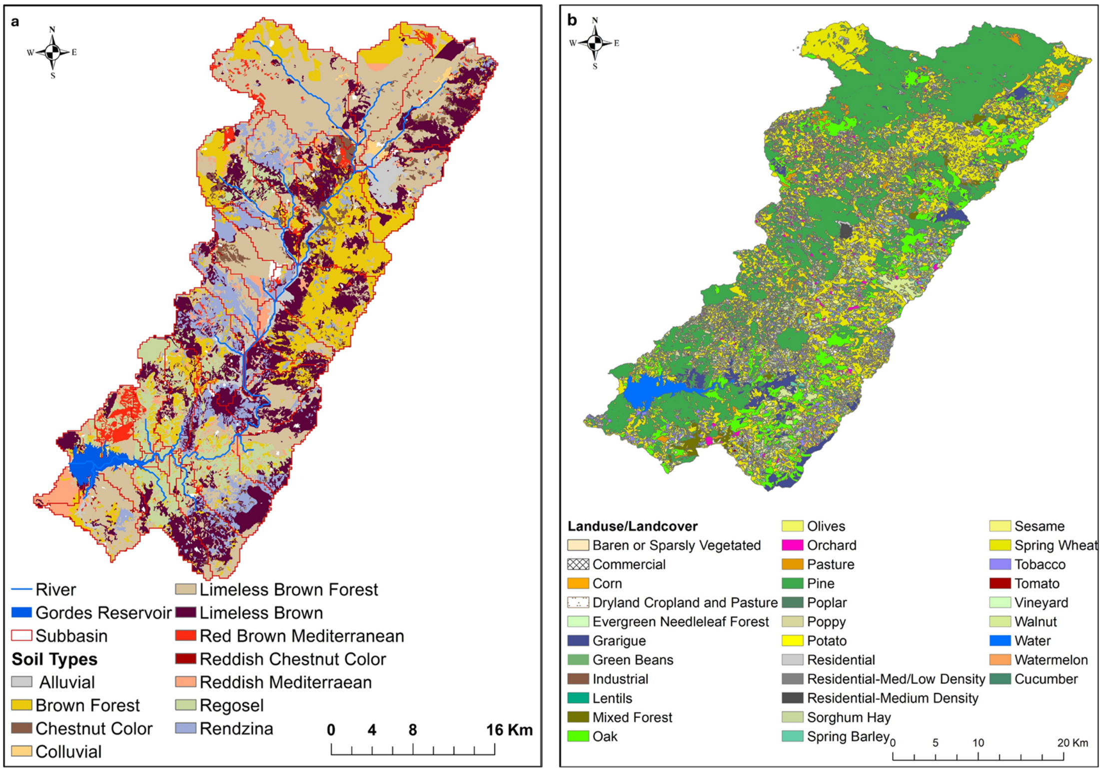

Figure 2. (**a**) Soil map and (**b**) land use/cover map of the study area.

There are about 150,000 sheep, 21,000 dairy cattle, and 62,000 chickens in the Gordes basin. Poultry farms produce little domestic wastewater as they use very little water during the production phase. The amount of wastewater produced in these facilities is added to the domestic wastewater section in the pollution load calculations [27]. Livestock manure is used as fertilizer to meet the needs of the crops grown in the catchment area, which partly causes non-point source pollution in the study area.

2.2. Model Description

SWAT was developed to quantify the effects of land management practices on catchment hydrology and water quality in medium to large river basins [28]. It is an agro-hydrological model that simulates weather, hydrology, erosion/sedimentation, plant growth, nitrogen, pesticides, and agricultural management at daily time steps [29]. In SWAT, sub-basins are divided based on topography and the river network. The sub-basins are further subdivided into hydrological response units (HRUs), where each unique combination of the underlying geographic maps (soils, land use, and slope) forms an individual HRU.

The land-phase processes in SWAT, including surface runoff and erosion processes, soil water movement, evapotranspiration, crop growth, and soil nitrogen cycling, are calculated at the HRU level and then aggregated for each sub-basin. The model estimates surface runoff using the Natural Resources Conservation Service Curve Number (NRCS) method [30], accounting for land use, the hydrologic soil type, and antecedent soil moisture. Percolation through each layer of soil is predicted using a storage routing technique combined with a crack flow model [31]. Evapotranspiration is estimated based on simulated soil moisture and plant water uptake and is limited to the potential evapotranspiration calculated using the equation of either (i) Priestley and Taylor [32], (ii) Penman and Monteith [33], or (iii) Hargreaves [34]. Plant growth is modelled by simulating leaf area development, light interception, and the conversion of intercepted light into biomass while taking into account stress due to extreme temperatures and water and nitrogen deficiencies. Nitrogen can be added to the soil through fertilizer, manure, or residue application, bacterial fixation, and rainfall. It can be removed from the soil via plant uptake, leaching, volatilization, denitrification, and erosion [35]. Soil erosion is calculated using the Modified Universal Soil Loss Equations—MUSLE [36]. SWAT considers a wide range of agricultural practices including tillage, fertilizer and manure application, tile drainage, and irrigation. Water withdrawals for irrigation or urban use can be considered from various sources, such as aquifers or directly from the stream [35].

The routing phase in SWAT can be defined as the movement of water, nutrients, and sediments through the channel network to the watershed outlet. Channel routing is represented by either the variable storage or Muskingum routing methods. Streamflow routing also includes the channel transmission losses of water, sediment settling and entrainment, and nitrogen degradation during transport [35].

The HRU generation approach in the SWAT model is based on user-defined thresholds, which have some drawbacks. Thresholds that are set too high may result in ignoring some important combinations that can have a major impact on the hydrologic processes in the watershed. On the other hand, if thresholds are set too low, a large number of HRUs can hinder good model parameterization and calibration. To overcome this problem, we used the methodology of Ozdemir et al. (2017) [26]. In this study, the combination of the HRU generation approach in the SWAT model and a hierarchical HRU approach was used to improve model performance and to not ignore important crops in the model when applying the hierarchical HRU approach (details are provided in the Supplementary Materials).

2.3. Model Inputs

The hydrological cycle of the basin was simulated in daily and monthly time steps. Daily time series data were used for all meteorological datasets (minimum and maximum temperature, precipitation, average relative humidity, average wind speed, and average solar radiation), while land use and soil types are spatial and static types of input data. The data and data properties used to set up the SWAT model of the Gordes Dam Basin are detailed in Table 1.

Table 1. Datasets used for SWAT model setup.

Data	Description	Data Source	Year	Scale
Hydrological	Streamflow	DSI monitoring station	1979–2018; missing data: 1997–2013	daily
Meteorological	Precipitation, temperature, humidity, solar radiation, and wind speed	NCEP/CFSR (The National Centers for Environmental Prediction/Climate Forecast System Reanalysis)	1974–2014	daily
DEM	Delineation of cells and the generation of a stream network	1/25,000 topographic map (Gordes 2017)		10 m
Land use map	Land use types	STATIP project map (Ministry of Agriculture and Forestry), supported crop products map obtained from T.C. General Directorate of Agriculture Reform, detailed forest map obtained from T.C. General Directorate of Forestry	2018	10 m
Soil map	Soil types and properties	Ministry of Agriculture and Forestry, and shape files		10 m
Pollution sources	Point and non-point pollution sources	Gordes Dam Basin Special Provision Determination, Gediz River Basin Management Plan Project		Kg/monthly
Climate change scenarios, RCP 4.5 and RCP 8.5	Precipitation and temperature	The General Directorate of Meteorology	2025–2097	daily

Due to the lack of local meteorological data in the basin, global meteorological datasets were used. NCEP/CFSR (The National Centers for Environmental Prediction/Climate Forecast System Reanalysis) data were used to obtain meteorological data for the study area, as the data provided satisfactory results in Turkey, where local meteorological time series have many gaps [24,37–40]. These data were combined with in situ measurements from several ground stations. The meteorological data processed from the station near the study area were from between 1979 and 2014 in the daily time step. A digital elevation model (DEM) with a grid cell resolution of 25 × 25 m, generated from a 1:25,000 topographic map, was used to delineate the catchment and the stream. The hydrological characteristics of the catchment were determined by evaluating the hydrological data of the Gordes stream, which was measured at the Hacihidir gauging station between 1979 and 1996. The maximum surface flow of the Gordes Stream was observed in December, January, March, and April as a result of surface recharge due to the onset of effective rainfall throughout the region and the melting of snow falling at higher elevations due to the warming of the climate. According to the monthly average flow values measured at the Gordes Stream gauging station over many years (1979–1996), the month with the highest flow is January, with 9.86 m^3/s, and the month with the lowest flow is August, with 0.063 m^3/s. According to the monthly measurements between 1979 and 1996, the average monthly discharge over many years is about 3.2 m^3/s.

The main soil physical and chemical properties needed to calculate hydrologic processes in SWAT are available soil water capacity, hydraulic conductivity, organic carbon content, soil texture (sand, silt, clay, and gravel content), and soil layer thickness. The soil map of the study area (scale: 1:25,000) obtained from the Ministry of Agriculture and Forestry of the Republic of Turkey does not include these properties and they had to be determined as follows. Soils in Turkey [41] were classified by the former Ministry of Food, Agriculture and Livestock according to their depth, salinity, slope, and drainage characteristics. The percentages of clay, sand, and silt content were defined based on the approach of Ardas and Creutberg (1995) [42] in Turkey using the depth and slope information of the soils. Soil texture was determined using the soil texture triangle [42]. The USLE equation soil erodibility (K) factor (USLE_K) was defined in relation to the soil textures. The available soil water capacity (SOL_AWC) was defined by using soil texture groups, as described in [43]. The soil bulk density (SOL_BD) values were defined based on soil texture groups by using the Guidelines for Soil Description (2006) [44]. Soil hydraulic conductivity (SOL_K) was determined using soil texture groups, as proposed in the Guidelines for Soil Description [44].

The land use map of the basin does not include the crops cultivated. Thus, a map of land use and land cover was created by merging a map of crops obtained from the General Directorate of Agriculture Reform, the STATIP project map, and a detailed forest map produced by the General Directorate of Forestry. The STATIP project data were produced using SPOT satellite data at 5 m and 2.5 m resolution on the 1:25,000 topographic map used for object-based classification (Figure 3).

According to data from the General Directorate of Agriculture Reform, the area of supported crops in the basin ranges from 161 to 472 km^2 for the years 2013–2020. The data show that the government has supported about 107 different types of crops. Based on the STATIP data, the supported crop types were identified and generalized. According to the new land use/land cover map produced, there are predominantly wheat and pine trees in the basin (Figure 2b). The map of supported crops for 2016 was chosen in combination with the STATIP data, as there were more supported areas for crop production in that year compared to previous years. In 2016, about 77 different crops received governmental support in the basin. These 77 crop types were generalized as much as possible to allow for an efficient model set-up and run time. The generalization was based on crop properties such as the harvest index. Because sesame and poppy are not included in the SWAT database, these crops were added after their crop parameters were defined based on other research studies [45–49]. For forest areas, each tree type was extracted individually from the detailed forest map of the General Directorate of Forestry. The location of water bodies and industrial, village, and urban areas was taken from the STATIP data. All of these datasets were combined with the crop pattern map to produce a land use/land cover map of the study area.

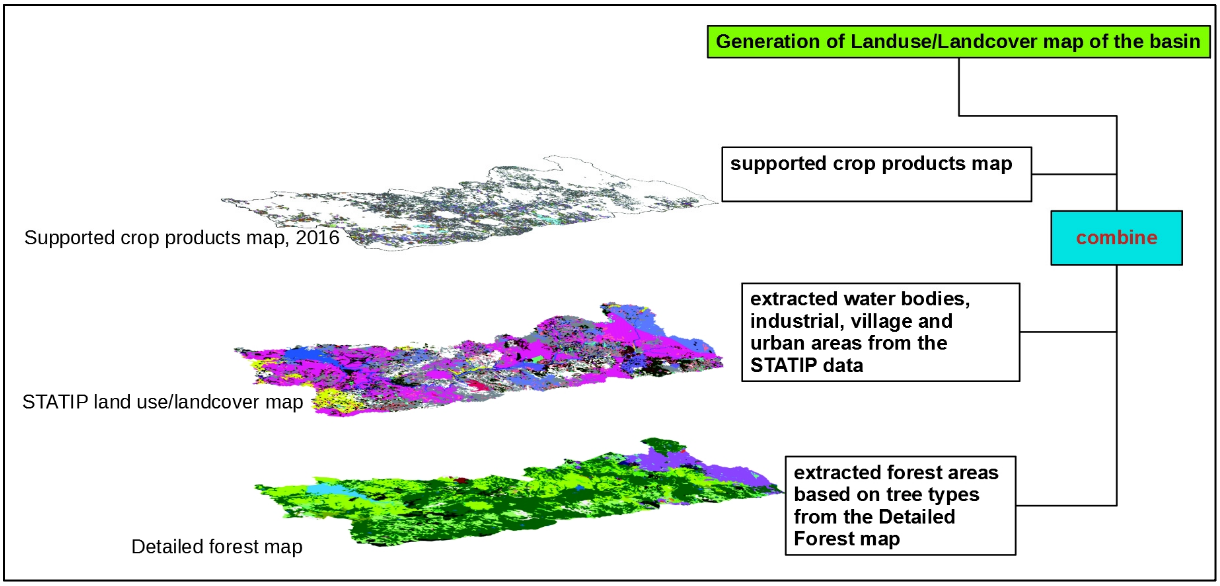

Figure 3. Steps for the generation of the land use and land cover map of the study area.

The economic relevance of crops in the basin was assessed based on TUIK (Turkish Statistical Institute) data for the years 2017, 2018, and 2019 to show that determining the most appropriate land use and management pattern can have important economic benefits. To assess the impacts of climate change on crops in the basin, we selected corn (CORN), potatoes (POTA), tobacco (TOBC), winter wheat (WWHT), winter barley (WBAR), poppy (POPY), cucumber (CUCM), sorghum hay (SGHY), and sesame (SESA) as they have the highest economic relevance in the basin. The selection was based on the data provided by the Manisa Provincial Directorate of Agriculture, whose mission is to define, implement, monitor, and evaluate innovative policies to ensure sustainable agricultural production, access to sufficient and safe food, rural development, and competitiveness. For the Gordes district, these are the most important crops, and their production costs are the highest.

Statistical approaches and estimates of fertilizer applications [50–52] often need to be used when spatially explicit fertilizer data are lacking [53]. Therefore, the amount of fertilizer applied to each crop in the basin was determined by taking into account the 'Manisa Agricultural Provincial Directorate Fertilizer' guidelines [54]. The fertilization recommendations of the guidelines are based on the analysis of P_2O_3 (kg/ha) and the percentage of organic matter in the soils of Manisa province. The excrements of the livestock in the basin are used as a fertilizer for poppy and potatoes according to a booklet for farmers published by the Provincial Directorate of Agriculture [54]. The amount of manure produced by poultry, cattle, and sheep was calculated using the animal pollution load coefficients proposed by Uttormark et al. (1974) [55]. In addition to the amount of fertilizer, the guidelines for farmers provided by the Ministry of Agriculture and Forestry also include agricultural management operations such as the timing of planting, harvesting, and irrigation for different types of cereals and other crops in the basins. Based on this information, relevant agricultural management operations were assigned to the SWAT model (Table 2).

Table 2. Agricultural management operation schedule in the basin.

Crop Type	Planting Time	Fertilizer Type (%N-%P_2O_5-%K_2O)	Fertilizer Time	Fertilizer Amount	Irrigation Time	Harvest Time
WWHT	15 October	18-46-00 46-00-00 46-00-00	15 October 1 February 1 March	155 kg/ha 100 kg/ha 100 kg/ha	15 October: Auto Irrigation 1 May: Auto Irrigation	30 June
TOBC	1 April	15-15-00 15-15-00 46-00-00	1 March 1 April 1 October	140 kg/ha 150 kg/ha 200 kg/ha	1 April: Auto Irrigation 15 April: Auto Irrigation 1 May: Auto Irrigation 15 May: Auto Irrigation 30 May: Auto Irrigation 15 June: Auto Irrigation 1 July: Auto Irrigation 15 July: Auto Irrigation 1 August: Auto Irrigation	20 August
POPPY	15 October	Continuous fertilization by using animal manure 18-46-00 Urea	30 August 10 September 16 October	Calculated based on animal numbers 150 kg/ha 40 kg/ha	15 October: Auto Irrigation 1 June: Auto Irrigation	30 July
SESA	1 May	15-15-00 15-15-00	3 March 1 May	200 kg/ha 200 kg/ha	1 May: Auto Irrigation 1 June: Auto Irrigation 1 July: Auto Irrigation 1 August: Auto Irrigation	30 September
WBAR	15 October	18-46-00 46-00-00 46-00-00	15 October 1 February 1 March	155 kg/ha 145 kg/ha 145 kg/ha	15 October: Auto Irrigation 1 May: Auto Irrigation	30 June
CORN	15 April	20-20-00 46-00-00	15 April 15 May	500 kg/ha 200 kg/ha	15 April: Auto Irrigation 30 April: Auto Irrigation 15 May: Auto Irrigation 30 May: Auto Irrigation 1 June: Auto Irrigation 15 June: Auto Irrigation 30 June: Auto Irrigation 7 July: Auto Irrigation 20 July: Auto Irrigation 1 August: Auto Irrigation	30 August
POTA	10 April	Urea 18-46-00 Continuous fertilization by using animal manure	10 April 1 May 30 March	200 kg/ha 100 kg/ha	10 April: Auto Irrigation 1 May: Auto Irrigation 1 June: Auto Irrigation 1 July: Auto Irrigation 1 August: Auto Irrigation 1 September: Auto Irrigation	30 October
SGHY	15 March	Urea 18-46-00 Urea	15 March 30 March 1 May	300 kg/ha 500 kg/ha 400 kg/ha	15 March: Auto Irrigation 20 April: Auto Irrigation 1 May: Auto Irrigation 20 May: Auto Irrigation 20 June: Auto Irrigation 1 July: Auto Irrigation	20 July
CUCM	10 May	10-20-20 Elemental nitrogen 33-00-00	1 May 15 May 25 May	500 kg/ha 400 kg/ha 140 kg/ha	30 May: Auto Irrigation 5 June: Auto Irrigation 10 June: Auto Irrigation 16 June: Auto Irrigation 20 June: Auto Irrigation 1 July: Auto Irrigation 5 July: Auto Irrigation 10 July: Auto Irrigation 20 July: Auto Irrigation 5 August: Auto Irrigation 10 August: Auto Irrigation 20 August: Auto Irrigation	30 August

There is only one water quality monitoring station in the basin. The measured parameters are chemical oxygen demand (COD) mg/L, biological oxygen demand (BOD) mg/L, ammonium–nitrogen (NH_4-N) mg/L, nitrite–nitrogen (NO_2-N) mg/L, nitrate–nitrogen (NO_3-N) mg/L, and suspended sediments (SS) mg/L. However, long-term continuous water quality measurements have not been carried out, and data availability is limited to bi-monthly measurements for the period of 2000–2004.

2.4. Model Setup and Calibration

The basic model setup was carried out using the input data described in Section 2.2 using the ArcGIS 10.7.1 interface [56] of SWAT2012. The DEM was used for the delineation of the catchment area and the provision of topographic parameters such as the length of the slope for each sub-catchment area. A total of 33 sub-basins were created based on the locations of livestock and their associated point sources (Figure 1). The SCS method was chosen to calculate surface runoff, and the asymmetric distribution was used to predict the distribution of precipitation. Potential evapotranspiration was calculated using the Penman–Monteith method. Monthly streamflow and nitrogen concentration data measured at the Hacihidir gauging station (Figure 1) were used for model calibration.

To identify the most sensitive parameters for model calibration, a sensitivity analysis was performed using the automatic sensitivity analysis tool implemented in SWAT [57]. These sensitive parameters were calibrated using a software package called Fast Automatic Calibration Tool (FACT). FACT was developed to improve the performance of automatic calibration procedures for SWAT models [58]. The optimization method used in FACT is the Sequential Uncertainty Conformity Algorithm (SUFI-2), as this algorithm can handle a large number of parameters and perform uncertainty analyses. FACT was developed to reduce some of the disadvantages of SUFI2 in SWAT-CUP that are time-consuming, such as the need for user interaction and problems with updating SWAT files [58]. The SUFI-2 algorithm [59,60] takes all parameter uncertainties (parameter, conceptual model, input, etc.) into account on the parameters (expressed as uniform distributions or ranges) and attempts to fit most of the measurement data within the 95% prediction uncertainty (95 PPU) of the model in an iterative process. To quantify the level of all uncertainties, the P-factor is used, which is the percentage of observed data bracketed by the 95% prediction uncertainty (95 PPU). The 95 PPU is calculated at the 2.5% and 97.5% levels of the cumulative distribution of the output variables using the Latin hypercube sampling method [60]. The R-factor, which reflects the average thickness of the 95 PPU band divided by the standard deviation of the measured data, is another index to quantify the strength of a calibration and uncertainty analysis. In theory, a P-factor of 1 and an R-factor of 0 indicate that the simulation is in exact agreement with the measurements [60,61].

In this study, the Nash–Sutcliffe coefficient of efficiency (NSE) [62] and the coefficient of determination (R^2) were used to compare the observed and measured values. The coefficient of determination (R^2) determines the degree of correlation between simulated and measured data. The coefficient of determination describes the proportion of variance in the data measured by the model, and its value ranges from 0 to 1 (Equation (1)). Higher values indicate less error variance, and typically, values greater than 0.5 are considered adequate. The NSE is a normalized statistic that determines the relative size of the variance in the measured data compared to the variance in the observed data (Equation (2)). The NSE indicates how well the plot of observed and simulated data fits the 1:1 line [62]. The NSE function represents not only the relationship between simulated and observed flow but also the evaluation of the water quantity bias. Model accuracy was evaluated based on the performance evaluation criteria of Moriasi et al. (2015) [63].

$$R^2 = \frac{\left[\sum_i \left(Q_{m,i} - \overline{Q}_m\right) \times \left(Q_{s,i} - \overline{Q}_s\right)\right]^2}{\sum_i \left(Q_{m,i} - \overline{Q}_m\right)^2 \times \sum_i \left(Q_{s,i} - \overline{Q}_s\right)^2} \tag{1}$$

$$\mathrm{NSE} = 1 - \frac{\sum_i (Q_m - Q_s)_i^2}{\sum_i \left(Q_{m,i} - \overline{Q}_m\right)^2} \quad (2)$$

$Q_{m,i}$—the observed value of the evaluated component at point i;
$\overline{Q}_m$—average of the observed value of the evaluated component;
$Q_{s,i}$—measured value of the evaluated component at point i;
$\overline{Q}_s$—average measured value of the evaluated component.

The hierarchical HRU approach and the HRU definition approach of SWAT were combined in order to reduce computational time and to not ignore crop patterns when defining the number of HRUs in SWAT. After applying the hierarchical approach to HRU division based on the method of Ozdemir et al. 2017 [26] (see the Supplementary Materials for details on the application procedure of HRU division in the model), eight HRUs (eight-HRU type; 187 HRUs were obtained) provided an optimum number of HRUs. Thus, the total target number of HRU types in ArcSWAT 2012.10_7.25 was set to 187 and exceptions to the land use threshold were defined for nine crops (CORN, POTA, TOBC, WWHT, WBAR, POPY, CUCM, SGHY, and SESA), pastures, forest areas, and olive trees. After defining the crop types in the HRU generation in ArcSWAT 2012.10_7.25, a total of 764 HRUs were generated for 33 sub-basins.

In the first step, the model was run for the period between 1979 and 1996 for the hydrological processes. In the second step, the simulation period was set to 1998–2014 with a two-year warm-up period, as water quality measurements were available for these years. The model results for hydrological processes were calibrated between 1979–1986 and validated between 1987–1996. The model results for nitrogen transport were calibrated between 2000–2005 and validated between 2006–2013.

2.5. Climate Change Scenarios

According to the Fifth Assessment Report (AR5) of the Intergovernmental Panel on Climate Change (IPCC 2014), representative concentration pathways (RCPs) are new scenarios based on global greenhouse gas and aerosol concentrations and alternative future scenarios as a starting point (SRES). General circulation models (GCMs) focus on RCPs for future climate projections [64]. The results of these studies have been widely used to investigate climate change impacts associated with the scenarios at regional and global scales [65]. These projections can be used to assess the impact of climate change on hydrological variables and crop growth parameters [14,66].

The General Directorate of Meteorology in Turkey has developed climate projections for the period of 2016–2097 using the global datasets HadGEM2-ES, MPI-ESM-MR, and GFDL-ESM2M to show how climate change will affect Turkey in the future. In this study, projection results were obtained at 20 km resolution with the reference period 1971–2000 and the future period of 2025–2097. The RegCM4.3.4 regional model and a dynamic downscaling method were used to downscale the RCP 4.5 and RCP 8.5 scenarios of the global models. The RCP 4.5 (540 ppm CO_2) and RCP 8.5 (940 ppm CO_2) scenarios were chosen to show the effects of future climate projections on the streamflow, nitrogen loads, and crop yields in the Gordes Dam basin. While RCP 4.5 defined the long-term level of moderate greenhouse gas concentrations as a broadly predefined forcing stabilization boundary, RCP 8.5 recognizes that greenhouse gas emissions will increase over time in the 21st century, approaching very high levels by 2100 [1]. Therefore, both a medium-emissions scenario (RCP 4.5) and a high-emissions scenario (RCP 8.5) were selected to assess a wide range of potential risks associated with the impacts of climate change.

3. Results and Discussion

3.1. Model Calibration

3.1.1. Hydrological Calibration

Parameters representing the associated hydrological processes, such as surface runoff, base flow, and lateral flow (Table 3), were calibrated by using FACT with 200 simulations.

Before choosing the calibration parameters, a sensitivity analysis was performed. The sensitivity analysis showed that the SCS runoff curve number (CN2) was the most sensitive parameter for the catchment. Parameters such as groundwater delay (GW_DELAY), baseflow alpha factor (ALPHA_BF), saturated hydraulic conductivity (SOL_K), and the available water capacity of the soil layer (SOL_AWC) also showed higher sensitivity to hydrological processes. After calibration and validation of the model for the hydrological process, the model achieved performance criteria of NSE = 0.84; R^2 = 0.85 and NSE = 0.70; R^2 = 0.71 (Figure 4a). The calibration model results can be considered "very good" with NSE and R^2 values greater than 0.80 based on the assessment of Moriasi et al. (2015) [63]. However, the validation results can be considered "good" and "satisfactory" with NSE and R^2 values greater than 0.7, respectively, based on the assessment of Moriasi et al. (2015) [63].

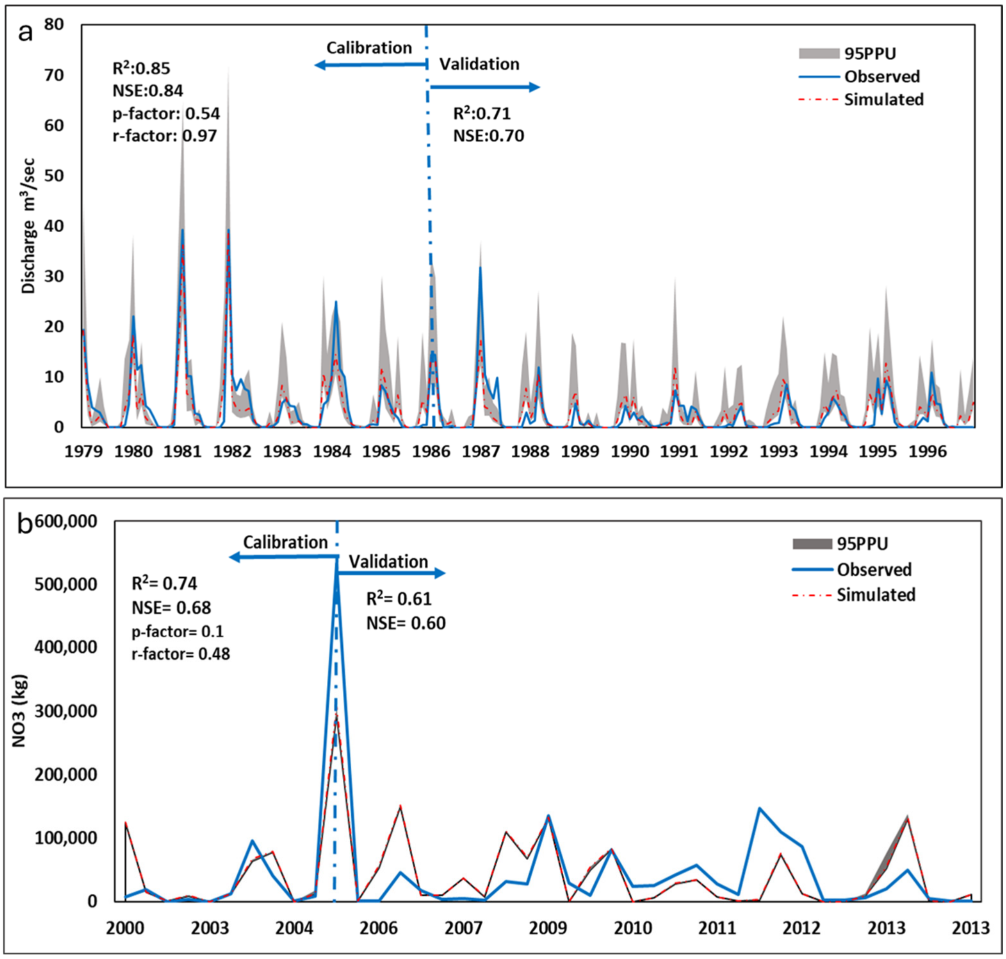

Figure 4. (**a**) Comparison of observed and simulated discharge and (**b**) comparation of observed and simulated nutrients.

Table 3. Calibration parameters for hydrological processes and their range (r__ refers to a relative change where the current values are multiplied by one plus a factor from the given parameter range, v__ refers to the substitution by a value from the given parameter range, a__ refers to the existing parameter value increased by a given value).

Parameters	Definition	Min–Max	Fitted Values	Process
r__CN2.mgt	Initial SCS runoff curve number	−0.2–0.2	−0.113	
r__SOL_AWC.sol	Available water capacity of the soil layer	−0.4–0.4	−0.01	Surface runoff
r__SOL_K.sol	Saturated hydraulic conductivity (mm/hr)	−0.4–0.4	−0.322	
v__ESCO.hru	Soil evaporation compensation factor.	0.8–1	0.9535	

Table 3. *Cont.*

Parameters	Definition	Min–Max	Fitted Values	Process
v__SURLAG.bsn	Surface runoff lag time	0.05–24	6.696125	Lateral flow
a__GWQMN.gw	The threshold depth of water in the shallow aquifer required for return flow to occur (mm H_2O)	0–25	24.062	
a__GW_REVAP.gw	Groundwater "revap" coefficient	−0.1–0	−0.02875	Base flow
v__REVAPMN.gw	Threshold depth of water in the shallow aquifer for "revap" or percolation to the deep aquifer to occur (mm H_2O)	0–500	201.25	
v__ALPHA_BF.gw	Baseflow alpha factor (days)	0–1	0.7575	
v__GW_DELAY.gw	Groundwater delay time (days)	30–450	35.25	
v__SFTMP.bsn	Snowfall temperature (°C)	−5.0–5.0	−4.525	
v__SMTMP.bsn	Snowmelt base temperature (°C)	−5.0–5.0	0.375	Snow
v__SMFMX.bsn	Melt factor for snow on 21 June (mm H_2O/°C-day)	0–10	2.375	
v__SMFMN.bsn	Melt factor for snow on 21 December (mm H_2O/°C-day)	0–10	0.825	
v__TIMP.bsn	Snowpack temperature lag factor	0.01–1	0.037225	
r__SOL_BD.sol	Moist bulk density (Mg/m^3 or g/cm^3)	−0.4–0.4	−0.322	Other

3.1.2. Nitrogen Transport Calibration

Prior to calibration, a sensitivity analysis was performed using SWAT-CUP (one-at-a-time method). The analysis showed that the compensation factor for soil evapotranspiration (RCN) and the parameter for the distribution of nitrogen uptake (N_UPDIS) were the most sensitive parameters. The initial organic N concentration in the soil layer (SOL_ORGN), the rate constant for the biological oxidation of NH3 (BC1_BSN), the rate constant for the hydrolysis of organic nitrogen to ammonia (BC3_BSN), and the fraction of porosity from which anions are excluded (ANION_E) were also found to be sensitive input parameters for nitrogen transport processes.

The sensitive parameters (Table 4) were used to calibrate the model. The nitrogen processes were calibrated using FACT with 200 simulations. The model performance for calibration and validation was NSE = 0.68; R^2 = 0.74 and NSE = 0.61; R = 0.60 (Figure 4b). According to Moriasi et al. (2015) [63], the results of the calibration model were categorized as "very good" and "good" as they had R^2 and NSE values of over 0.70 and 0.60, respectively. However, the validation results were categorized as "good" as they had NSE and R^2 values of over 0.6.

Table 4. Calibration parameters for nitrogen transport, v__ refers to the substitution by a value from the given parameter range.

Explanation	Parameter	Min–Max	Fitted Values
Soil evaporation compensation factor	v__RCN.bsn	0–15	10.6125
Nitrogen uptake distribution parameter	v__N_UPDIS.bsn	0–100	88.75
Initial organic N concentration in the soil layer	v__SOL_ORGN().chm	0–100	99.75
Rate constant for the biological oxidation of NH3 (1/dayy)	v__BC1_BSN.bsn	0.1–1.0	0.21025
Rate constant for the hydrolysis of organic nitrogen to ammonia (1/dayy)	v__BC3_BSN.bsn	0.02–0.4	0.37435
Fraction of porosity from which anions are excluded	v__ANION_E.bsn	0.01–1	0.685675

"P-factor" and "R-factor" [59] are two indices represent uncertainty in the SUFI2 algorithm. AP-factor of 1 and an R-factor of 0 mean that the simulation agrees with the measured data. For the hydrological calibration procedures, the P-factor was 0.54 and the R-factor was 0.97 (Figure 4a). The catchment area of the Gordes Dam basin has a varied topography. In the high areas of the catchment, the inflows of the Gordes River are controlled by the snowmelt. This is reflected in the regular spring peaks and the near-zero discharges in the winter months. The increase in precipitation was important for recording the peak discharges in spring and summer. SWAT collects precipitation as snow in autumn/winter and melts it in spring/summer. Given the topographical differences in the catchment, it is surprising that the model can still simulate runoff so accurately at this location (NSE = 0.84; R^2 = 0.85), albeit with a small P-factor (0.54) and r-factor (0.97). For the nutrient calibration, the P-factor was 0.1 and the R-factor was 0.47.Although the accuracy of the nutrient transport in the model is "very good" and "good", the lack of data and the non-continuous water quality data are the reasons for the small P-factor (0.1) and R-factor (0.47).

3.1.3. Crop Yield Calibration

The plant growth parameters listed in Table 5 were used to calibrate crop yields for winter wheat (WWHT), winter barley (WBAR), corn (CORN), cucumber (CUCM), sesame (SESA), sorghum hay (SGHY), poppy (POPY), tobacco (TOBC), and potato (POTA). The sensitivity analysis for the crop yield parameters was performed manually (one by one for each crop). In addition, relevant information from several studies was used to define the most important parameters (e.g., [67–70]). The model was manually calibrated based on crop yields for the period of 2004–2013 using the sensitive plant growth parameters and observed yields (Table 5).

Table 5. Crop yield calibration parameters and their values before and after the calibration process (parameter values, HU, T_opt, etc., show the values before calibration; Cal: values obtained after calibration).

Crop	HU	Cal	T_opt	Cal	T_base	Cal	BIO_E	Cal	HVSTI	Cal	BLAI	Cal	WSYF	Cal
WWHT	1100	1300	18	18	0	4	30	30	0.4	0.52	4	3.2	0.2	0.3
WBAR	1200	1400	18	19	0	5	30	28	0.54	0.4	4	3	0.2	0.2
CORN	1537	1000	25	22	7	7	39	46	0.6	0.75	6	4.5	0.3	0.75
CUCM	800	600	32	26	16	12	30	38	0.27	0.8	1.5	3.5	0.25	0.3
SESA	1800	2000	25	25	10	10	30	30	0.35	0.35	3.5	3.5	0.2	0.2
SGHY	800	700	30	22	11	9	33.5	42	0.9	0.95	4	4.8	0.9	0.95
POPY	1800	2000	21	23	5	7	33	30	0.4	0.32	4.5	4.0	0.12	0.2
TOBC	1800	1900	25	22	10	10	39	38	0.55	0.5	4.5	4.0	0.55	0.4
POTA	1457	1050	22	22	7	8	25	34	0.95	1.1	4	4.5	0.95	0.95

Notes: HU: cumulative heat unit, T_opt: optimal temp for plant growth, T_base: min temp plant growth, BIO_E: biomass/energy ratio, HVSTI: harvest index, BLAI: max leaf area index, and WSYF: lower limit of the harvest index.

After crop yield calibration, the simulated and observed values of TOBC, WBAR, WWHT, SESA, and POPY were in close agreement with the available data for median, maximum, and minimum yields. The simulated yields of WBAR, TOBC, and POPY contain outliers. When evaluating the calibration crop yields, the calibration performance for SESA and WWHT yields was good. Although the median of the simulated and observed yields of POTA and SGHY are in perfect agreement, the maximum and minimum yields between the observed and simulated data are not in close agreement. The simulated and observed yields of CORN and CUCM were not in agreement during the calibration process. The CUCM yield was estimated to be lower based on the observed data. The TUIK database, from which the observed crop yield data were taken, contains district values, and the areas of each district within the study area are not within the boundaries of the study area. As a result, the simulated crop yields in the basin could be lower or higher than the observed yields. In addition, as cucumbers are harvested continuously, it was not possible to measure the exact cucumber yield. The observed cucumber yield does not reflect the actual yield in the field, as the cucumber yield is measured by the number of cucumber plants are sold based on TUIK data (Figure 5).

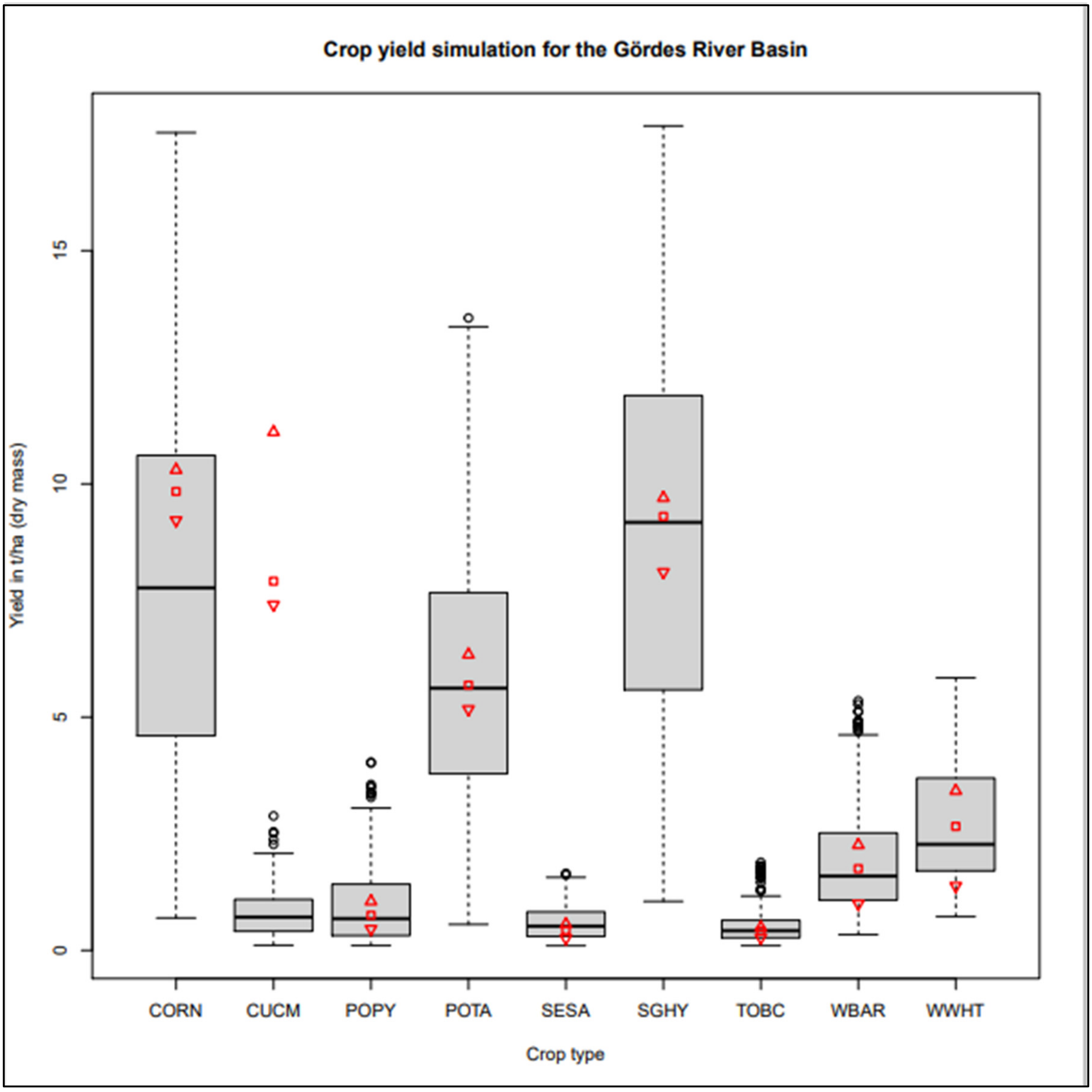

Figure 5. Calibration results of crop yields in the Gordes basin (red symbols: measured crop yields; boxes: simulated crop yields, black circle: outlier).

3.2. *Climate Change Scenarios*

The effects of climate change on streamflow, nitrogen transport, and crop yield were predicted by running the hydrological model under RCP 4.5 and RCP 8.5 scenarios between 2028 and 2060. The assessment of climate change impacts was carried out on the basis of 10-year steps. The downscaling of global models to a regional scale can be subject to a number of uncertainties due to a variety of factors. To obtain regional data, historical data were used to downscale the global model. However, there is a lack of data and continuity in the historical data, which leads to uncertainties in projecting future conditions. In addition, not all historical data could represent meteorological conditions everywhere in the catchment, as the catchment has a variety of topographical differences. The accuracy and reliability of the downscaled regional model may be affected by these uncertainties.

3.2.1. Climate Signal

According to the reference period, the average temperature in the basin is 14.8 °C and the average monthly precipitation is 1.7 mm/d. Maximum temperatures are recorded between June and August (Figure 6a). Maximum precipitation events occur from January to February according to the reference period (Table 6, Figure 6b). The average monthly precipitation and mean temperature changes of the RCP 4.5 and RCP 8.5 scenarios for the period of 2031–2060 were compared with the period of 1979–2013 to identify differences in future climate change. Although the increase in average monthly precipitation is similar for the RCP 4.5 and RCP 8.5 scenarios, it is projected to increase by 6.2 and 7 mm/year for the period of 2041–2050 under the RCP 4.5 and RCP 8.5 scenarios, respectively. For the period of 2051–2060, it is projected to increase by 6.4 and 5.4 mm/year under RCP 4.5 and RCP 8.5, respectively. Although more precipitation is measured between October and February for 1979–2013, more precipitation events are predicted between April and June for 2031–2060 under the RCP 4.5 and RCP 8.5 scenarios. More precipitation events are predicted in May and June under RCP 8.5 for 2041–2050. Average monthly precipitation is projected to be higher under RCP 4.5 for the period of 2031–2040 compared to the other scenario periods. Compared to temperature measurements for 1979–2014, the average temperature will increase by 1.3 °C under RCP 4.5 and 1.7 °C under RCP 8.5 (Table 6).

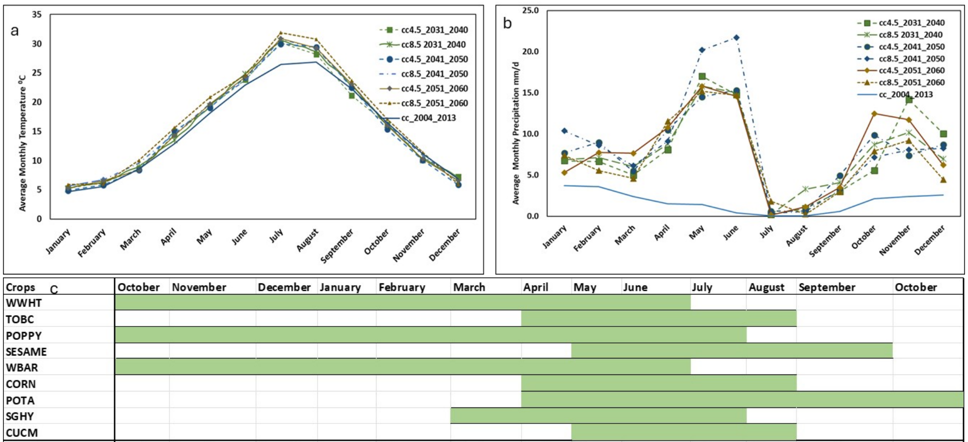

d Scenarios	October	November	December	January	February	March	April	May	June	July	August	September	October
cc_2004_2014	16.52	11.13	6.88	4.68	5.56	8.53	12.88	18.10	22.93	26.47	26.86	22.22	16.52
cc_2004_2014	2.12	2.41	2.56	3.74	3.59	2.40	1.52	1.41	0.41	0.06	0.03	0.57	2.12
cc4.5_2031_2040	16.20	10.05	7.26	5.27	6.21	8.61	14.39	19.23	23.86	30.15	28.19	21.15	16.20
cc4.5_2041_2050	15.36	10.07	5.86	4.86	5.81	8.41	15.07	19.06	24.22	29.96	29.43	22.47	15.36
cc4.5_2051_2060	15.97	10.30	6.58	5.27	6.52	8.38	14.29	19.70	24.31	30.89	29.27	23.10	15.97
cc4.5_2031_2040	8.72	10.18	6.96	6.88	7.15	6.01	8.77	15.79	15.00	0.24	3.28	4.09	8.72
cc4.5_2041_2050	7.17	8.06	8.24	10.37	8.60	6.13	9.10	20.21	21.73	0.36	0.60	3.18	7.17
cc4.5_2051_2060	7.92	9.20	4.45	7.40	5.54	4.61	11.52	15.19	14.72	1.80	0.24	2.95	7.92
cc8.5 2031_2040	16.21	10.30	7.11	5.10	6.33	8.95	13.52	19.33	24.80	30.50	28.78	22.72	16.21
cc8.5_2041_2050	16.27	10.85	6.48	5.66	6.69	9.55	14.60	19.75	23.68	30.88	29.11	22.98	16.27
cc8.5_2051_2060	17.11	11.40	5.94	5.89	6.04	10.03	15.64	20.84	24.65	31.90	30.77	23.70	17.11
cc8.5 2031_2040	8.72	10.18	6.96	6.88	7.15	6.01	8.77	15.79	15.00	0.24	3.28	4.09	8.72
cc8.5_2041_2050	7.17	8.06	8.24	10.37	8.60	6.13	9.10	20.21	21.73	0.36	0.60	3.18	7.17
cc8.5_2051_2060	7.92	9.20	4.45	7.40	5.54	4.61	11.52	15.19	14.72	1.80	0.24	2.95	7.92

Figure 6. (**a**) Temperature and (**b**) precipitation values under climate change scenarios RCP 4.5 and RCP 8.5 based on the sub-periods of 2031–2060; (**c**) planting and harvest time of each crop; (**d**) table of average monthly temperature and precipitation values based on sub-periods of climate change scenarios (blue color: average monthly precipitation (mm/month); orange color: average mean monthly temperature °C; green color: planting and harvesting period of each crop).

Table 6. The results of RCP 4.5 and RCP 8.5 climate change scenarios on streamflow and nitrogen loads.

+/−Indicates Change; Values in "()" Indicate Prediction				
Meteorological prediction	**1979–2014**	**2031–2040**	**2041–2050**	**2051–2060**
RCP 4.5 Avg Temperature (°C)		+1.2 (16)	+1.2 (16)	+1.4 (16.2)
RCP 8.5 Avg Temperature (°C)		+1.3 (16.1)	+1.6 (16.4)	+2.2 (17)
RCP 4.5 Avg Precipitation (mm/d)		+6 (7.7)	+6.2 (7.9)	+6.4 (8.1)
RCP 8.5 Avg Precipitation (mm/d)		+6 (7.7)	+7 (8.7)	+5.4 (7.1)
Temperature Avg (°C)	14.8			
Precipitation (mm/d)	1.7			
Streamflow m^3/s				

Table 6. *Cont.*

+/−Indicates Change; Values in "()" Indicate Prediction				
Scenarios	**1979–1996**	**2031–2040**	**2041–2050**	**2051–2060**
RCP 4.5		+1.1 (4.4)	+2.5 (5.7)	+2.5 (5.7)
RCP 8.5		+1.2 (4.4)	+4 (7.2)	+0.7 (3.9)
Reference period	3.2			
Nitrogen t/year				
Scenarios	**2004–2013**	**2031–2040**	**2041–2050**	**2051–2060**
RCP 4.5		+8.8 (25.1)	+13.5 (29.8)	+25.1 (41.4)
RCP 8.5		+12.3 (28.6)	+16.5 (32.8)	+15.7 (32)
Reference period	16.3			

3.2.2. Hydrology

Under RCP 4.5, the long-term mean streamflow was predicted to be 4.43, 5.72, and 5.73 m^3/s for the periods of 2031–2040, 2041–2050, and 2051–2060, respectively. Under the RCP 8.5 scenario, the mean streamflow was predicted to be 4.4, 7.24, and 3.9 m^3/s for the same periods. The projected change in the precipitation regime, i.e., an increase in precipitation from April to July compared to the other months under RCP 4.5 and RCP 8.5, could lead to an increase in streamflow. The response of the stream to the change in precipitation regime in the study area, which is influenced by the steep slopes of the study area, can lead to higher streamflow values. The time it takes for precipitation to reach the river as runoff may vary due to changes in topographic elevation and basin shape. For the periods of 2031–2040 and 2041–2050, a greater increase in streamflow is projected under RCP 8.5 than under RCP 4.5 compared to the measured streamflow of 3.2 m^3/s for 1979–1996. In addition, for the period of 2051–2060, streamflow is projected to increase significantly by 2.5 m^3/s (predicted value: 5.7 m^3/s) under RCP 4.5 compared to RCP 8.5 (+0.7; 3.9 m^3/s). The period of 2041–2050 is projected to have the largest increase in streamflow under RCP 8.5 (Table 6).

When analyzing the impact of climate change (RCP. 4.5 and RCP 8.5) on the discharge of the Gordes Dam based on monthly data for the period of 2041–2050, the predicted discharge from February to April is higher than the discharge of the reference period (1979–2014). From February to April, the predicted discharge is also higher than at any other time of the year (Figure 4a). However, for the period of 2031–2040, the discharge from March to May is predicted to be higher than in the other months. For the period of 2051–2060, the discharge from March to May is predicted to decrease compared to current climate conditions, while the discharge from June to December is predicted to increase (Figure 7a). The results show that the catchment is no longer facing water shortages.

3.2.3. Nitrogen

Under RCP 4.5, the nitrogen loads for the periods of 2031–2040, 2041–2050, and 2051–2060 were predicted to be 25.1, 29.8, and 41.4 t/year, respectively (Table 6). The nitrogen loads based on RCP 8.5 for the same periods were predicted to be 28.6, 32.8, and 32 t/year, respectively (Table 6). The nitrogen loads for 2051–2060 are expected to be lower than for 2041–2050 under RCP 8.5. The maximum increase in nitrogen loads is projected to occur between 2041 and 2050 under RCP 8.5. Although nitrogen loads are projected to be higher under RCP 8.5 than under RCP 4.5, the maximum increase in nitrogen loads is projected to occur between 2051 and 2060 under RCP 4.5. Based on the increase in streamflow for the 2031–2040 and 2041–2050 periods under RCP 8.5, the nitrogen loads are projected to be higher than under RCP 4.5. Under RCP 8.5, nitrogen loads are projected to be higher from February to April in 2041–2050 than in other periods. However, RCP 4.5 and RCP 8.5 for the period of 2031–2040 show that nitrogen loads are projected to be high from March to May. Although RCP 4.5 and RCP 8.5 for the period of 2051–2060 predict low nitrogen loads for February and March compared to current climate conditions, the nitrogen loads for the same period from April to December are projected to be high (Figure 7b).

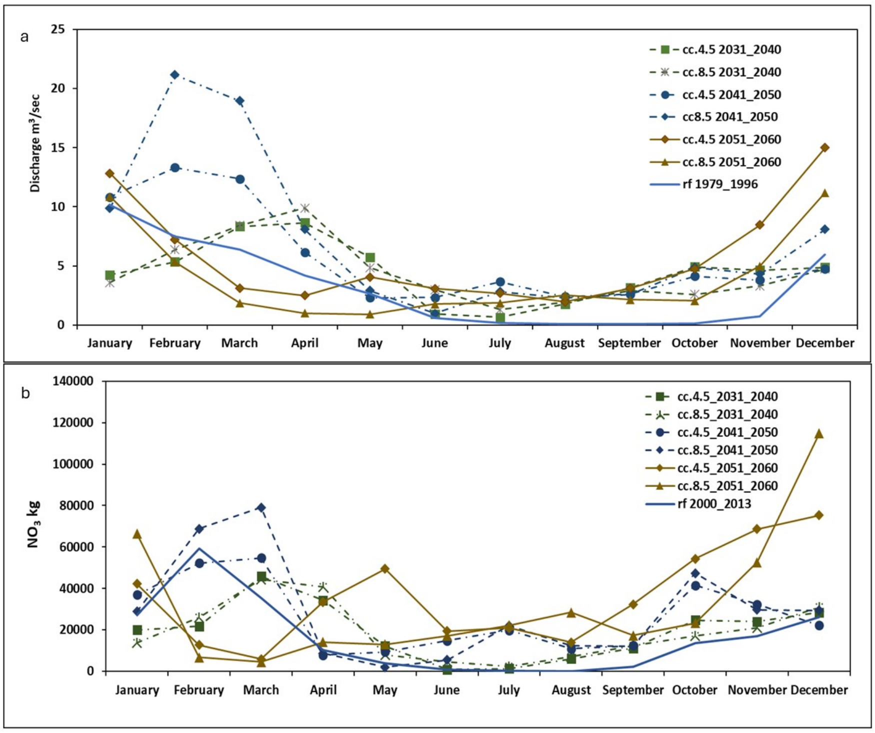

Figure 7. (**a**) Effects of RCP 4.5 and RCP 8.5 climate change scenarios on streamflow; (**b**) Effects of RCP 4.5 and RCP 8.5 climate change scenarios on nitrogen loads (rf: reference period; cc: climate change, e.g., cc.4.5 shows climate change RCP 4.5).

3.2.4. Crop Yields

The average monthly temperature and precipitation for the period between planting and harvest of each crop were compared with the climate change sub-periods and the historical period to understand the impact of climate change on crop yields (Figure 6). According to RCP 4.5, the average monthly temperature is expected to increase from February to August. The maximum temperature increase from 2051 to 2060 under RCP 4.5 is projected to be higher than in other years. However, the average monthly temperature is projected to decrease in November, December, January, and October under RCP 4.5. Although the situation is expected to be the same under RCP 8.5, the average temperature is predicted to be higher under RCP 8.5 than under RCP 4.5, and the temperature in October and November is expected to increase more under RCP 8.5 than under RCP 4.5 for the period of 2051–2060 (Figure 6a,d). Compared to the historical period of 2003–2014, average monthly precipitation from November to April is expected to decrease under RCP 4.5. However, precipitation is predicted to increase from April to June under RCP 4.5. Although the precipitation pattern projections under RCP 8.5 are similar to those under RCP 4.5, the change will be more dramatic (Figure 6b,d).

The effects of climate change on the crop yields of CORN, CUCM, POPY, POTA, SESA, SGHY, TOBC, WBAR, and WWHT were investigated based on RCP 4.5 and RCP 8.5 scenarios. As the historical crop yield data belong to the period of 2004–2013, crop yield comparisons were made for the periods of 2031–2040, 2041–2050, and 2051–2060 (Figure 8). The impact of climate change on crop yields shows that some crops would be positively affected in some periods while others would be negatively affected. For example, in some periods, rising temperatures and changing rainfall patterns may lead to higher yields for certain crops such as POPY, SESA, and TOBC in the basin. Climate change is expected to have a negative impact on CORN, POTA, CUCM, and SGHY. The average corn yield is predicted to be the same for the RCP 4.5 2041–2050 and RCP 8.5 2031–2040 periods. According to the scenarios for CORN, its yield will decrease compared to the historical period. Heat stress often occurs during the summer season (July and August), and studies have shown that yield may decrease due to higher temperatures above 32.5 °C [71]. To obtain adequate CORN yields under changing climatic conditions, it is necessary either to change the sowing and harvesting dates for corn seed germination under conditions where the soil temperature is around 10 °C or to plant an appropriate corn type that is resistant to severe and mild water stress.

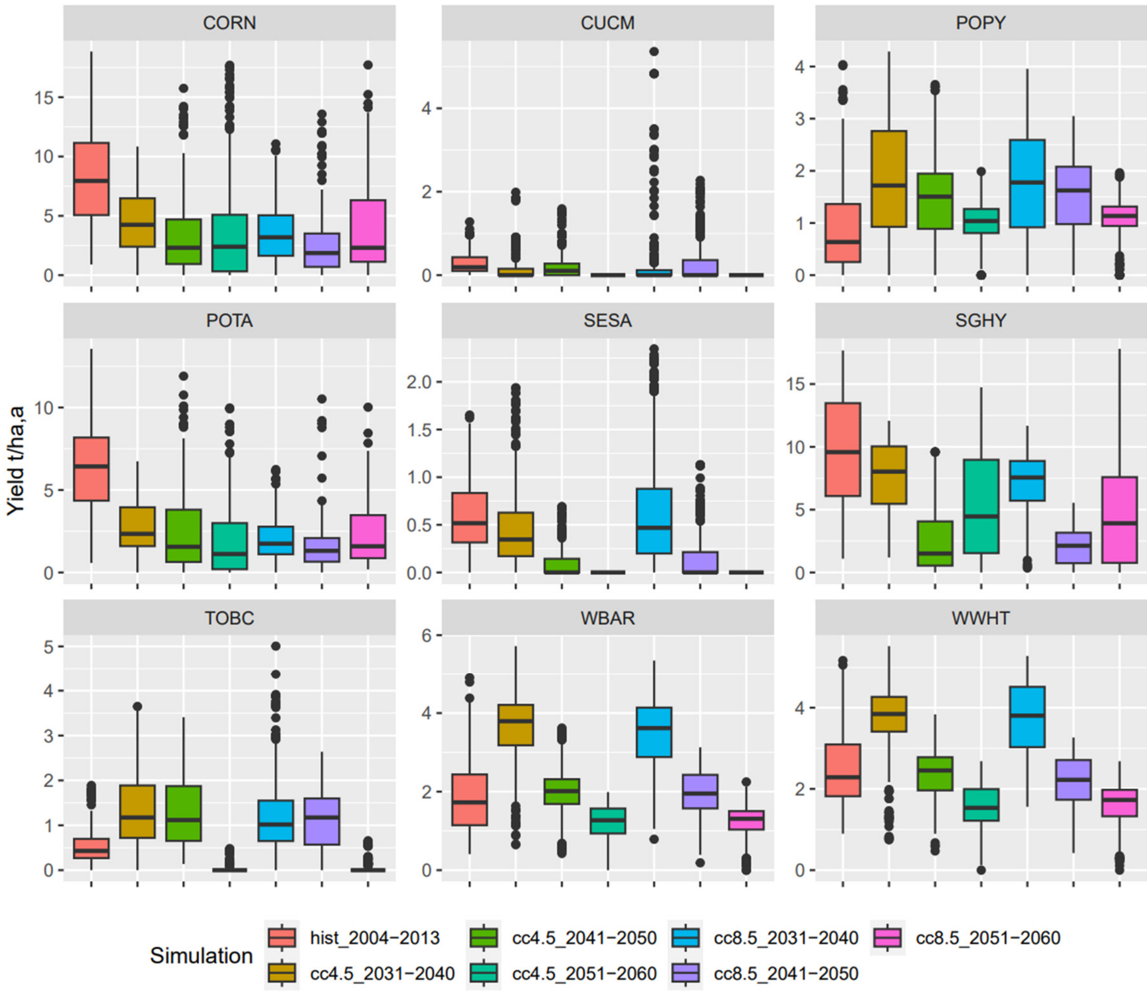

Figure 8. Climate change impacts on crop yields under the RCP 4.5 and RCP 8.5 climate change scenarios (black circle: outlier).

CUCM is likely to be dramatically affected by changing climate conditions. CUCM thrives in warm temperatures and require a relatively stable environment to grow and produce fruit. If temperatures are too high, CUCM plants can experience heat stress, which can lead to reduced yields, poor fruit quality, and even plant death. In addition to temperature, cucumbers are also sensitive to changes in water availability. They require consistent moisture throughout the growing season, but excessive rainfall or drought can be detrimental to plant health and yield [72]. CUCM should be replaced by crops that are tolerant to water and heat stress.

Predictions of POPY yields based on climate change scenarios show that yields will increase. However, the POPY yield for the RCP 4.5 2031–2040 and 2041–2050 and RCP 8.5 2031–2040 and 2041–2050 periods will be twice that of the other periods. The October and July poppy planting and harvesting seasons are expected to be positively influenced in terms of yield by changes in precipitation and temperature (Figure 6c,d).

The SESA yield will decrease based on the RCP 4.5 2041–2050 and 2051–2060 and RCP 8.5 2041–50 and 2051–2060 periods, and the SESA yield will increase for the RCP 8.5 2031–2040 period. According to the comparison with the historical period, the SESA yield in the RCP 4.5 2031–2040 period will be about the same as in the historical period (Figure 8). According to the RCP 8.5 scenario for the period of 2031–2040, precipitation will increase in May and have a stable pattern through June, unlike the other periods in the scenarios (Figure 6). The mean temperature will also increase more between May and August than in other months. This increase and the stable rainfall pattern between May and June, the SESA growing season, are expected to have a positive impact on SESA yields.

The POTA yield for RCP 4.5 2041–2050 and 2051–2060 is predicted to be the same as for RCP 8.5 2051–2060. If the POTA yield simulated in the climate change scenarios is compared to historical periods, the average potato yield will decrease by about three times. Changing rainfall patterns and rising temperatures will dramatically reduce POTA yields. The optimum temperature range for POTA growth is about 15–21 °C. Both high temperatures and excessive rainfall can negatively affect potato yields by reducing the size and quality of the tubers produced [73]. It is therefore important to monitor and manage these environmental factors to optimize POTA yields.

The SGHY yield is predicted to decrease based on the climate change scenarios; however, the maximum SGHY yield is expected to be approximately the same for RCP 4.5 2031–2040 and 2051–2060 and RCP 8.5 2031–2040 and 2051–2060. The average SGHY yield based on the RCP 4.5 and 8.5 scenarios for the period of 2031–2040 is expected to be unchanged. Changes in precipitation patterns and increases in temperature are predicted to have a negative impact on SGHY. Although SGHY is a drought-tolerant plant, it still requires a certain amount of water to grow and thrive [74]. Extreme temperatures and changes in rainfall patterns can affect SGHY yields [75]. For example, extreme heat can damage the photosynthetic system of plants, reducing their ability to produce biomass [76]. Overall, climate change is likely to have a negative impact on SGHY yields, with potentially significant implications for livestock production and food security. Strategies such as improved irrigation techniques and the development of drought-tolerant sorghum varieties may be needed to mitigate these effects.

Climate change based on RCP 4.5 2031–2040 and RCP 8.5 2031–2040 will have a positive effect on TOBC; climate change based on RCP 4.5 and 8.5 scenarios for 2051–2060 will have a negative effect on TOBC; the yield of TOBC will be almost zero after this period. If TOBC is planted in April and harvested in August, with a temperature increase of about 2 °C based on the RCP 4.5 and RCP 8.5 scenarios for 2031–2040 and 2041–2050, and an increase in precipitation in April and May, the yield of TOBC is expected to increase. However, TOBC yield is predicted to be negatively affected by climate change under the RCP 4.5 and RCP 8.5 scenarios for the 2051–2060 period, as temperature and precipitation would increase more than in other periods during the TOBC planting period (Figure 7). While increases in temperature and precipitation can potentially lead to higher TOBC yields, prolonged droughts or extreme weather events such as floods and storms can lead to reduced yields and poor-quality TOBC [77].

Although WBAR is expected to be negatively affected by climate change based on RCP 4.5 and RCP 8.5 for 2041–2050, the yield of WBAR based on RCP 4.5 and RCP 8.5 for 2031–2040 will be higher than in the other scenarios and the historical period. When considering the impact of climate change on WWHT, the situation is similar to that of WBAR. However, according to the RCP 8.5 2031–2040 period for WWHT, the yield of this crop will be approximately higher than WBAR (Figure 8). In contrast with WBAR, WWHT is predicted to have higher yields based on climate change scenarios. Some studies suggest that WWHT may be more resilient to climate change than winter barley and may even have higher yields under certain climate change scenarios [78]. One reason is that winter wheat has a longer growing season than WBAR, giving it a better chance to take advantage of favorable weather conditions. In addition, WWHT has a higher tolerance to heat stress and can recover from drought better than WBAR [79]. Some climate change models also predict increased precipitation in some areas, which could be beneficial for winter wheat [80]. WWHT and WBAR are planted in October and harvested in June. According to the RCP 4.5 and RCP 8.5 scenarios for 2031–2040, WWHT and WBAR are expected to have higher yields than in other periods. Between the planting and harvesting periods of WBAR and WWHT, the temperature will increase by about 3–4% under RCP 4.5 and RCP 8.5 2031–2040. This increase could lead to an increase in the yield of these crops (Figure 8).

Although the limited availability of data on factors such as water quality, crop yields, etc., can lead to uncertainties in model results and overconfidence in the predicted impacts of climate change on streamflow, nitrogen loads, and crop yields, SWAT is able to demonstrate good model performance in the ungauged catchments [63,81,82]. According to Hoang et al. 2019 study [83], the integration of the water quality model QUAL2K and SWAT shows good results for model performance in the case of gaps in water quality data. SWAT-EC (a modified version of SWAT2012 referred to as SWAT-EC) achieved better results in improving model performance in ungauged catchments for understanding and assessing the impacts of agricultural conservation practices, land use change, and climate adaptation measures on water quality in large river basins [84].

4. Conclusions

This study aims to show the impacts of climate change on streamflow, nitrogen load, and crop yield in the Gordes Dam Basin, a sub-basin of the Gediz Basin. In this study, the SWAT model was set up with a hierarchical HRU division approach and used to simulate the climate change scenarios RCP 4.5 and RCP 8.5 to assist decision-makers in identifying the most appropriate land use and management pattern for the present and future in the Gordes Dam Basin. The combination of the hierarchical approach and SWAT's current definitions of HRUs ensures that crop patterns are not ignored when defining HRUs in SWAT while reducing computational time.

According to the RCP 4.5 and RCP 8.5 scenarios, the average temperature is expected to increase by about 1.2 to 2.2 °C, and precipitation is expected to increase by almost 6 mm/d on average. In addition, the pattern of the precipitation regime will change according to the climate change scenarios, with an increase in precipitation between April and June, in contrast with the historical precipitation pattern. For the periods of 2031–2040, 2041–2050, and 2051–2060, the RCP 4.5 projections show significant increases in streamflow of between 1.1 and 2.5 m^3/s. Under RCP 8.5, streamflow is projected to increase by 1.2, 4, and 0.7 for the 2031–2040, 2041–2050, and 2051–2060 periods, respectively. Under RCP 4.5, nitrogen loads are projected to increase by about 8.8 and 25.1 t/year. Under RCP 8.5, nitrogen loads are projected to increase by 12.3, 16.5, and 15.7 t/year for the 2031–2040, 2041–2050, and 2051–2060 periods, respectively. Appropriate water and land management policies should be applied to ensure sustainable water management. Rising temperatures may lead to a change in precipitation from snow to rain in winter. They could also lead to earlier snowmelt in spring.

Appropriate cropping patterns that are tolerant to changing climatic conditions should be developed to mitigate the impacts of climate change on crop production and sustain economic development. POPY, SESA, TOBC, WBAR, and WWHT can be supported under RCP 4.5 for the 2031–2040 period and RCP 8.5 for the 2031–2040 and 2041–2050 periods. POPY and SGHY may be supported under RCP 4.5 for the 2031–2040 and 2051–2060 periods and RCP 8.5 for the 2041–2050 and 2051–2060 periods. TOBC for the 2031–2040 and 2041–2050 periods can be supported based on both climate change scenarios. According to the climate change scenarios, CORN, CUCM, and POTA are predicted to be negatively affected by climate change. If these crops are to be grown, the sowing time can be changed to improve germination and flowering conditions. In addition, appropriate varieties of these crops that are tolerant to changing climatic conditions should be selected.

It is important to note that while some crops may benefit from climate change in the short term, the long-term consequences could be disastrous for global agriculture and food security. The negative impact of climate change on crop yields, combined with other factors such as population growth, land use change, and resource depletion, could lead to food shortages and higher food prices in many regions, with significant social and economic consequences. It is therefore vital that we take action to mitigate the effects of climate change on agriculture and develop sustainable agricultural practices that can adapt to changing climate conditions. The planting and harvesting times of crops should be changed according to changing rainfall and temperature patterns. It is possible to grow products with high resistance to changing climate patterns.

A new dam or pond may be built in the basin to capture excess water during high-flow periods for use during drought or low-flow periods. In addition, the increased streamflow will promote natural water storage and infiltration through the restoration of wetlands, floodplains, and other natural areas. These ecosystems can help slow and absorb excess water, reducing the risk of flooding and improving water quality. Implementing nitrogen management practices in agricultural areas, such as reducing the amount or timing of fertilizer application, can help reduce nitrogen runoff and protect water quality. Restoring natural areas, such as wetlands or riparian buffers, can help filter and absorb nitrogen from runoff, reducing nitrogen loads in waterways. Policymakers should integrate climate change adaptation considerations into nitrogen management plans and water resource management strategies. Adaptation measures should be implemented to address changing nitrogen dynamics. Policymakers should encourage farmers to adopt climate-smart agricultural practices that minimize soil erosion, improve water retention, and enhance nitrogen cycling.

Although data gaps in water quality and crop yields led to uncertainties in this study, it could be valuable for decision-makers in the basin to develop appropriate land and water management policies. This study was able to show the best management practices in the basin. However, it could not fully show the changes in water quality and quantity and the ecological balance of the changed land use and management pattern for economic benefits. In further studies, the model should be combined with optimization methods to show the most suitable cropping pattern to protect water resources and the environment and provide economic benefits.

Supplementary Materials: The following supporting information can be downloaded at: https://www.mdpi.com/article/10.3390/w16101371/s1. Figure S1. General concept of the hierarchical methodology (Ozdemir et al., 2017) [26]. Figure S2. HRU generation by combining CN2, soil hydraulic conductivity, and slope classification. Table S1. Summary flow results of HRU division for the Gordes Dam.

Author Contributions: All authors contributed to the study conception and design. Conceptualization, A.Ö. and M.V.; data curation, A.Ö.; formal analysis, A.Ö., M.S. and F.W.; funding acquisition, A.Ö.; methodology, A.Ö.; project administration, A.Ö.; resources, A.Ö.; software, A.Ö. and M.S.; supervision, M.V.; validation, A.Ö.; writing—original draft, A.Ö.; writing—review and editing, A.Ö., M.V., M.S. and F.W. All authors have read and agreed to the published version of the manuscript.

Funding: This work was supported by TUBITAK (grant number 2219). Author Ayfer OZDEMIR has received research support from TUBITAK.

Data Availability Statement: Data will be made available upon request.

Acknowledgments: We would like to thank TUBITAK (Scientific and Technological Research Council of Turkey) for providing partial support for this research. We are thankful to Şekip Erdal and Semiha Kiremitci for their support in evaluating the agricultural management of corn and sorghum hay in this study. We would also like to thank Tugba Uysal for her help in determining the fertilizer applications.

Conflicts of Interest: The authors declare that they have no known competing financial interests or personal relationships that could have appeared to have influenced the work reported in this paper.

References

1. IPCC. *Climate Change 2014: Synthesis Report. Contribution of Working Groups I, II and III to the Fifth Assessment Report of the Intergovernmental Panel on Climate Change*; Core Writing Team, Pachauri, R.K., Meyer, L.A., Eds.; IPCC: Geneva, Switzerland, 2014; p. 151.
2. Liu, Q.; Niu, J.; Sivakumar, B.; Ding, R.; Li, S. Accessing future crop yield and crop water productivity over the Heihe River basin in northwest China under a changing climate. *Geosci. Lett.* **2021**, *8*, 2–16. [CrossRef]
3. Chen, Y.; Marek, G.W.; Marek, T.H.; Porter, D.O.; Brauer, D.K.; Srinivasan, R. Simulating the effects of agricultural production practices on water conservation and crop yields using an improved SWAT model in the Texas High Plains, USA. *Agric. Water Manag.* **2021**, *244*, 106574. [CrossRef]
4. Papadopoulos, T.; Balta, M.E. Climate Change and big data analytics: Challenges and opportunities. *Int. J. Inf. Manag.* **2022**, *63*, 102448. [CrossRef]
5. IPCC; Ali, E.; Cramer, W.; Carnicer, J.; Georgopoulou, E.; Hilmi, N.J.M.; Le Cozannet, G.; Lionello, P. Cross-Chapter Paper 4: Mediterranean Region. In *Climate Change 2022: Impacts, Adaptation and Vulnerability. Contribution of Working Group II to the Sixth Assessment Report of the Intergovernmental Panel on Climate Change*; Pörtner, H.-O., Roberts, D.C., Tignor, M., Poloczanska, E.S., Mintenbeck, K., Alegría, A., Craig, M., Langsdorf, S., Löschke, S., Möller, V., et al., Eds.; Cambridge University Press: Cambridge, UK; New York, NY, USA, 2020; pp. 2233–2272. [CrossRef]
6. Erol, A.; Randhir, T.O. Climatic change impacts on the ecohydrology of Mediterranean watersheds. *Clim. Change* **2012**, *114*, 319–341. [CrossRef]
7. Christensen, J.H.; Kanikicharla, K.K.; Aldrian, E.; An, S.I.; Cavalcanti, I.F.A.; de Castro, M.; Dong, W.; Goswami, P.; Hall, A.; Kanyanga, J.K.; et al. Climate Phenomena and Their Relevance for Future Regional Climate Change. In *Climate Change 2013 the Physical Science Basis: Working Group I Contribution to the Fifth Assessment Report of the Intergovernmental Panel on Climate Change*; Cambridge University Press: Cambridge, UK, 2013; pp. 1217–1308.
8. Coppens, J.; Trolle, D.; Jeppesen, E.; Beklioğlu, M. The impact of climate change on a Mediterranean shallow lake: Insights based on catchment and lake modelling. *Reg. Environ. Change* **2020**, *20*, 62. [CrossRef]
9. Ertugrul, M.; Varol, T.; Ozel, H.B.; Cetin, M.; Sevik, H. Influence of climatic factor of changes in forest fire danger and fire season length in Turkey. *Environ. Monit. Assess.* **2021**, *193*, 28. [CrossRef]
10. Demircan, M.; Gürkan, H.; Eskioğlu, O.; Arabacı, H.; Coşkun, M. Climate Change Projections for Turkey: Three Models and Two Scenarios. *Turk. J. Water Sci. Manag.* **2017**, *1*, 22–43. [CrossRef]
11. Lionello, P.; Malanotte-Rizzoli, P.; Boscolo, R.; Alpert, P.; Artale, V.; Li, L.; Xoplaki, E. The Mediterranean climate: An overview of the main characteristics and issues. *Dev. Earth Environ. Sci.* **2006**, *4*, 1–26.
12. Sen, Z. *Climate Change, Droughts, and Water Resources. Applied Drought Modeling, Prediction, and Mitigation*; Elsevier: Amsterdam, The Netherlands, 2015; pp. 321–391.
13. Michaelides, S.; Karacostas, T.; Sánchez, J.L.; Retalis, A.; Pytharoulis, I.; Homar, V.; Nisantzi, A. Reviews and perspectives of high impact atmospheric processes in the Mediterranean. *Atmos. Res.* **2018**, *208*, 4–44. [CrossRef]
14. Gorguner, M.; Kavvas, M.L.; Ishida, K. Assessing the impacts of future climate change on the hydroclimatology of the Gediz Basin in Turkey by using dynamically downscaled CMIP5 projections. *Sci. Total Environ.* **2019**, *648*, 481–499. [CrossRef]
15. Kirdemir, U.; Okkan, U.; Fistikoglu, O. Projecting aridity from statistically downscaled and bias-corrected variables for the Gediz Basin, Turkey. *J. Water Clim. Change* **2022**, *13*, 3061–3082. [CrossRef]
16. Gorguner, M.; Kavvas, M.L. Modeling impacts of future climate change on reservoir storages and irrigation water demands in a Mediterranean basin. *Sci. Total Environ.* **2020**, *748*, 141246. [CrossRef]
17. Ozcan, A.; Strauss, E. An Overview of the Impacts of Global Climate Change on Farmland in Turkey. *Int. J. Environ. Sci. Dev.* **2016**, *7*, 458–463. [CrossRef]
18. Bucak, T.; Trolle, D.; Tavşanoğlu, Ü.N.; Çakıroğlu, A.İ.; Özen, A.; Jeppesen, E.; Beklioğlu, M. Modeling the effects of climatic and land use changes on phytoplankton and water quality of the largest Turkish freshwater lake: Lake Beyşehir. *Sci. Total Environ.* **2018**, *621*, 802–816. [CrossRef]
19. Dudu, H.; Çakmak, E.H. Climate change and agriculture: An integrated approach to evaluate economy-wide effects for Turkey. *Clim. Dev.* **2018**, *10*, 275–288. [CrossRef]
20. Chandio, A.A.; Ozturk, I.; Akram, W.; Ahmad, F.; Mirani, A.A. Empirical analysis of climate change factors affecting cereal yield: Evidence from Turkey. *Environ. Sci. Pollut. Res.* **2020**, *27*, 11944–11957. [CrossRef]
21. Kumanlioglu, A.A. Characterizing meteorological and hydrological droughts: A case study of the Gediz River Basin, Turkey. *Meteorol. Appl.* **2020**, *27*, e1857. [CrossRef]
22. Yerdelen, C.; Abdelkader, M.; Eris, E. Assessment of drought in SPI series using continuous wavelet analysis for Gediz Basin, Turkey. *Atmos. Res.* **2021**, *260*, 105687. [CrossRef]
23. Tan, G.; Shibasaki, R. Global estimation of crop productivity and the impacts of global warming by GIS and EPIC integration. *Ecol. Model.* **2003**, *168*, 357–370. [CrossRef]
24. Wang, K.; Onodera, S.; Saito, M.; Okuda, N.; Okubo, T. Estimation of Phosphorus Transport Influenced by Climate Change in a Rice Paddy Catchment Using SWAT. *Int. J. Environ. Res.* **2021**, *15*, 759–772. [CrossRef]
25. Shahvari, N.; Khalilian, S.; Mosavi, S.H.; Mortazavi, S.A. Assessing climate change impacts on water resources and crop yield: A case study of Varamin plain basin, Iran. *Environ. Monit. Assess.* **2019**, *191*, 134. [CrossRef]

26. Ozdemir, A.; Leloğlu, U.M.; Abbaspour, K. Hierarchical Approach to Hydrological Model Calibration. *Environ. Earth Sci.* **2017**, *76*, 318. [CrossRef]
27. Gördes PDWU. The Gördes Dam Basin Special Provisions. 04.07.2017/310. 2017. Available online: https://www.tarimorman.gov.tr/SYGM/Belgeler/i%C3%A7me%20suyu%20koruma%20planlar%C4%B1/G%C3%B6rdes%20Baraj%20G%C3%B6l%C3%BC%20%C3%96zel%20H%C3%BCk%C3%BCmleri.pdf (accessed on 28 August 2017).
28. Arnold, J.G.; Fohrer, N. SWAT2000: Current capabilities and research opportunities in applied watershed modelling. *Hydrol. Process* **2005**, *19*, 563–572. [CrossRef]
29. Cakir, R.; Sauvage, S.; Gerino, M.; Volk, M.; Sánchez-Pérez, J.M. Assessment of ecological function indicators related to nitrate under multiple human stressors in a large watershed. *Ecol. Indic.* **2020**, *111*, 106016. [CrossRef]
30. SCD. *Handbook of Hydrology*; Soil Conservation Department, Ministry of Agriculture: New Delhi, India, 1972.
31. Arnold, J.G.; Williams, J.R.; Maidment, D.R. Continuous-Time Water and Sediment-Routing Model for Large Basins. *J. Hydraul. Eng.* **1995**, *121*, 171–183. [CrossRef]
32. Priestley, C.; Taylor, R. On the assessment of surface heat flux and evaporation using large-scale parameters. *Mon. Weather Rev.* **1972**, *100*, 81–92. [CrossRef]
33. Monteith, J.L. Evaporation and environment. In *Symposia of the Society for Experimental Biology*; Cambridge University Press (CUP): Cambridge, UK, 1965; Volume 19, pp. 205–234.
34. Hargreaves, G.; Riley, J. Agricultural benefits for Senegal River basin. *J. Irrig. Drain. E-ASCE* **1985**, *111*, 113–124. [CrossRef]
35. Neitsch, S.L.; Arnold, J.G.; Kiniry, J.R.; Williams, J.R. *Soil & Water Assessment Tool Theoretical Documentation Version 2009*; (TR-406); Texas Water Resources Institute: College Station, TX, USA, 2011; pp. 1–647.
36. Williams, J.; Berndt, H. Sediment yield prediction based on watershed hydrology. *Trans. ASAE* **1977**, *20*, 1100–1104. [CrossRef]
37. Cuceloglu, G.; Ozturk, I. Assessing the Impact of CFSR and Local Climate Datasets on Hydrological Modeling Performance in the Mountainous Black Sea Catchment. *Water* **2019**, *11*, 2277. [CrossRef]
38. Karakoyun, E.; Kaya, N. Hydrological simulation and prediction of soil erosion using the SWAT model in a mountainous watershed: A case study of Murat River Basin, Turkey. *J. Hydroinform.* **2022**, *24*, 1175–1193. [CrossRef]
39. Ozdemir, A. Defining Groundwater Resources Protection Zones in Aquifers Using Stable Isotope Analysis: A Case Study from the Namazgah Dam Basin in Turkey. *Environ. Earth Sci.* **2019**, *78*, 509. [CrossRef]
40. Ozdemir, A. Determination of protection zones in drinking water basins: A case study from Turkey, Sapanca Lake Basin. *Environ. Earth Sci.* **2020**, *79*, 178. [CrossRef]
41. Oakes, H. *Türkiye Toprakları*; Türk Yüksek Ziraat Mühendisleri Birliği: İzmir, Turkey, 1958; Volume 18, 224p.
42. Ardas, S.; Creutzberg, D. *Soil Reference Profiles of Turkey*; Country Report 3; Department of Soil Science-Faculty of Agriculture-Çukurova University, International Soil Reference and Information Centre: Adana, Turkey, 1995.
43. Ley, T.W.; Stevens, R.G.; Topielec, R.R.; Neibling, W.H.; Soil Water Monitoring and Measurement. Pacific Northwest Cooperative Extension Bulletin—PNW0475. December 1994. Available online: http://irrigation.wsu.edu/Content/Fact-Sheets/Soil-Monitoring-and-Measurement.pdf (accessed on 30 August 2006).
44. Jahn, R.; Blume, H.P.; Asio, V.B.; Spaargaren, O.; Schad, P. *Guidelines for Soil Description*, 4th ed.; Food and Agriculture Organization of the United Nations: Rome, Italy, 2006; pp. 67–77.
45. Jahan, M.; Nassiri Mahallati, M.; Amiri, M.B.; Ehyayi, H.R. Radiation absorption and use efficiency of sesame as affected by biofertilizers inoculation in a low input cropping system. *Ind. Crops Prod.* **2013**, *43*, 606–611. [CrossRef]
46. Koocheki, A.; Mahallati, M.N.; Solouki, H.; Karbor, S. Evaluation of radiation absorption and use efficiency in substitution intercropping of sesame (*Sesamum indicum* L.) and mung bean (*Vigna radiata* L.). *Adv. Plants Agric. Res.* **2016**, *3*, 145–154.
47. Gloaguen, R.M.; Couch, A.; Rowland, D.L.; Bennett, J.; Hochmuth, G.; Langham, D.R.; Brym, Z.T. Root life history of non-dehiscent sesame (*Sesamum indicum* L.) cultivars and the relationship with canopy development. *Field Crops Res.* **2019**, *241*, 107560. [CrossRef]
48. Baydar, H. Susam (*Sesamum indicum* L.) çeşitlerinin agronomik, fizyolojik ve teknolojik özellikleri. *Süleyman Demirel Üniv. Bilim. Enst. Derg.* **2001**, *5*, 39–48.
49. Baydar, H. Susamda (*Sesamum indicum* L.) Verim, Yağ, Oleik ve Linoleik Tipi Hatların Tarımsal ve Teknolojik Özellikleri. *Akdeniz Univ. J. Fac. Agric.* **2005**, *18*, 267–272. Available online: https://dergipark.org.tr/tr/pub/akdenizfderg/issue/1580/19621 (accessed on 23 September 2005).
50. Villalobos, F.J.; Delgado, A.; López-Bernal, Á.; Quemada, M. FertiliCalc: A Decision Support System for Fertilizer Management. *Int. J. Plant Prod.* **2020**, *14*, 299–308. [CrossRef]
51. Bijay-Singh; Craswell, E. Fertilizers and nitrate pollution of surface and ground water: An increasingly pervasive global problem. *SN Appl. Sci.* **2021**, *3*, 518. [CrossRef]
52. Beza, M.; Hailu, H.; Teferi, G. Modeling and Assessing Surface Water Potential Using Combined SWAT Model and Spatial Proximity Regionalization Technique for Ungauged Subwatershed of Jewuha Watershed, Awash Basin, Ethiopia. *Adv. Civ. Eng.* **2023**, *2023*, 9972801. [CrossRef]
53. Volk, M.; Hirschfeld, J.; Dehnhardt, A.; Schmidt, G.; Bohn, C.; Liersch, S.; Gassman, P.W. Integrated ecological-economic modelling of water pollution abatement management options in the Upper Ems River Basin. *Ecol. Econ.* **2008**, *66*, 66–76. [CrossRef]
54. Gulec, H.; Pilanali, N.; Kalinbacak, K.; Kececi, M.; Ozcan, H. *Gubreleme Rehberi*; Tarim ve Orman Bakanligi: Ankara, Türkiye, 2018; pp. 1–30.

55. Uttormark, P.D.; Chapin, J.D.; Green, K.M. *Estimating Nutrient Loading of Lakes from Non-Point Sources*; Environmental Protection Agency Publication 660/3-74-020; U.S. Government Printing Office: Washington, DC, USA, 1974.
56. Winchell, M.; Srinivasan, R.; Di Luzio, M.; Arnold, J. *ArcSWAT Interface for SWAT2005 User's Guide*; Texas Agricultural Experiment 30 Station and United States Department of Agriculture: Temple, TX, USA, 2007.
57. Van Griensven, A.; Meixner, T.; Grunwald, S.; Bishop, T.; Diluzio, M.; Srinivasan, R. A global sensitivity analysis tool for the parameters of multi-variable catchment models. *J. Hydrol.* **2006**, *324*, 10–23. [CrossRef]
58. Ozdemir, A.; Leloğlu, U.M. A Fast and Automated Hydrologic Calibration Tool For SWAT. *Water Environ. J.* **2018**, *33*, 488–498. [CrossRef]
59. Abbaspour, K.C.; Johnson, C.A.; Van Genuchten, M.T. Estimating uncertain flow and transport parameters using a sequential uncertainty fitting procedure. *Vadose Zone J.* **2004**, *3*, 1340–1352. [CrossRef]
60. Abbaspour, K.C.; Yang, J.; Maximov, I.; Siber, R.; Bogner, K.; Mieleitner, J.; Zobrist, J.; Srinivasan, R. Modelling hydrology and water quality in the pre-alpine/alpine Thur watershed using SWAT. *J. Hydrol.* **2007**, *333*, 413–430. [CrossRef]
61. Abbaspour, K.C. *SWAT Calibration and Uncertainty Programs: A User Mannual*; Swiss Federal Institute of Aquatic Science and Technology (Eawag): Dübendorf, Switzerland, 2011.
62. Nash, J.E.; Sutcliffe, J.V. River flow forecasting through conceptual models, part 1—A discussion of principles. *J. Hydrol.* **1970**, *10*, 282–290. [CrossRef]
63. Moriasi, D.; Gitau, M.; Pai, N.; Daggupati, P. Hydrologic and Water Quality Models: Performance Measures and Evaluation Criteria. *Trans. ASABE (Am. Soc. Agric. Biol. Eng.)* **2015**, *58*, 1763–1785.
64. Rogelj, J.; Meinshausen, M.; Knutti, R. Global warming under old and new scenarios using IPCC climate sensitivity range estimates. *Nat. Clim. Change* **2012**, *2*, 248–253. [CrossRef]
65. Zhang, Y.; Wang, Y.; Niu, H. Effects of temperature, precipitation and carbon dioxide concentrations on the requirements for crop irrigation water in China under future climate scenarios. *Sci. Total Environ.* **2019**, *656*, 373–387. [CrossRef]
66. Zhang, H.; Väliranta, M.; Swindles, G.T.; Lopez, M.A.; Mullan, D.; Tan, N.; Amesbury, M.; Babeshko, K.V.; Bao, K.; Bobrov, A.; et al. Recent climate change has driven divergent hydrological shifts in high-latitude peatlands. *Nat. Commun.* **2022**, *13*, 4959. [CrossRef]
67. Musyoka, F.K.; Strauss, P.; Zhao, G.; Srinivasan, R.; Kalik, A. Multi-Step Calibration Approach for SWAT Model Using Soil Moisture and Crop Yields in a Small Agricultural Catchment. *Water* **2021**, *13*, 2238. [CrossRef]
68. Karki, R.; Srivastava, P.; Bosch, D.D.; Kalin, L.; Lamba, J.; Strickland, T.C. Multi-Variable Sensitivity Analysis, Calibration, and Validation of a Field-Scale SWAT Model: Building Stakeholder Trust in Hydrologic and Water Quality Modeling. *Trans. ASABE* **2020**, *63*, 523–539. [CrossRef]
69. Malik, W.; Isla, R.; Dechmi, F. DSSAT-CERES-maize modelling to improve irrigation and nitrogen management practices under Mediterranean conditions. *Agric. Water Manag.* **2019**, *213*, 298–308. [CrossRef]
70. Abbaspour, K.C.; Rouholahnejad, E.; Vaghefi, S.; Srinivasan, R.; Yang, H.; Kløve, B. A continental-scale hydrology and water quality model for Europe: Calibration and uncertainty of a high-resolution large-scale SWAT model. *J. Hydrol.* **2015**, *524*, 733–752. [CrossRef]
71. Crafts-Brandner, S.J.; Salvucci, M.E. Sensitivity of Photosynthesis in a C4 Plant, Maize, to Heat Stress. *Plant Physiol.* **2002**, *129*, 1773–1780. [CrossRef] [PubMed]
72. Kumar, R.; Reddy, K.M. Impact of Climate Change on Cucurbitaceous Vegetables in Relation to Increasing Temperature and Drought. In *Advances in Research on Vegetable Production Under a Changing Climate 1. Advances in Olericulture*; Solankey, S.S., Kumari, M., Kumar, M., Eds.; Springer: Cham, Switzerland, 2021.
73. Haverkort, A.J.; Franke, A.C.; Engelbrecht, F.A.; Steyn, J.M. Climate Change and Potato Production in Contrasting South African Agro-ecosystems 1. Effects on Land and Water Use Efficiencies. *Potato Res.* **2013**, *56*, 31–50. [CrossRef]
74. Hatfield, J.L.; Prueger, J.H. Temperature extremes: Effect on plant growth and development. *Weather Clim. Extrem.* **2015**, *10*, 4–10. [CrossRef]
75. Tsegaye, A.; Bergvinson, D. Climate change impacts and adaptation strategies for sorghum and millet production in developing countries. *J. SAT Agric. Res.* **2013**, *11*, 1–16.
76. Kamara, A.Y.; Ekeleme, F.; Tarawali, S.A. Climate change and variability: Implications for crop production, food security and livestock in West Africa. *Agric. Food Secur.* **2015**, *4*, 19.
77. Novotny, T.E.; Bialous, S.A.; Burt, L.; Curtis, C.; Iqtidar, S.U.; Liu, Y.; Pujari, S. The environmental and health impacts of tobacco agriculture, cigarette manufacture and consumption. *Bull. World Health Organ.* **2015**, *93*, 877–880. [CrossRef]
78. Wang, X.; Ji, Y.; Zhou, G.; Wang, S.; Yao, X. Climate Suitability and Vulnerability of Winter Wheat Planting in Gansu under the Background of Global Warming. *J. Geosci. Environ. Prot.* **2019**, *7*, 239–250. [CrossRef]
79. Musyimi, J.K.; Sinclair, F.L.; Ng'ang'a, J.K.; Muchugi, A. A systematic review of the impacts of climate variability and change on agroforestry systems in Africa. *Agric. Ecosyst. Environ.* **2018**, *258*, 148–159.
80. Xu, Y.; Li, T.; Xu, M.; Tan, L.; Shen, S. Assessing Climate Change Effects on Winter Wheat Production in the 3H Plain: Insights from Bias-Corrected CMIP6 Projections. *Agriculture* **2024**, *14*, 469. [CrossRef]
81. Arnold, J.G.; Srinivasan, R.; Muttiah, R.S.; Williams, J.R. Large area hydrologic modeling modeling and assessment Part I: Model development. *J. Am. Water Resour. Assoc.* **1998**, *34*, 73–89. [CrossRef]

82. Mapes, K.L.; Pricope, N.G. Evaluating SWAT Model Performance for Runoff, Percolation, and Sediment Loss Estimation in Low-Gradient Watersheds of the Atlantic Coastal Plain. *Hydrology* **2020**, *7*, 21. [CrossRef]
83. Hoang, B.H.; Hien, H.N.; Dinh, N.T.N.; Thao, N.A.; Ha, P.T.T.; Kandasamy, J.; Nguyen, T.V. Integration of SWAT and QUAL2K for water quality modeling in a data scarce basin of Cau River basin in Vietnam. *Ecohydrol. Hydrobiol.* **2019**, *19*, 210–223.
84. Qi, J.; Zhang, X.; Yang, Q.; Srinivasan, R.; Arnold, J.G.; Li, J.; Cole, J. SWAT Ungauged: Water Quality Modeling in the Upper Mississippi River Basin. *J. Hydrol.* **2020**, *584*, 124601. [CrossRef]

Disclaimer/Publisher's Note: The statements, opinions and data contained in all publications are solely those of the individual author(s) and contributor(s) and not of MDPI and/or the editor(s). MDPI and/or the editor(s) disclaim responsibility for any injury to people or property resulting from any ideas, methods, instructions or products referred to in the content.